An Analysis Method of Gas Absorption Spectrum Characteristics Based on Fuzzy Comprehensive Evaluation

Zhaocong Wu, Mingliang Li, Keyi Rao, Yixian Yue, and Anquan Xia

***Abstract*—The growing demand for atmospheric environment monitoring requires a more precise analysis of gas absorption spectral characteristics and simulation of radiation transfer within the absorption window. However, there is still a lack of clarity regarding the methods and technical details for extracting, analyzing absorption spectral characteristics, and simulating radiative transfer. This article proposes a fuzzy comprehensive evaluation method to analyze the impact on the absorption spectral characteristics of a gas and constructs a technical framework called spectrum characteristics analysis technical framework (SCATF) for atmospheric remote sensing detection. First, this article investigates the extraction method of the absorption window based on the HITRAN database. Then, it establishes the improved fuzzy comprehensive evaluation model (IFCE) for evaluating the absorption channel. Subsequently, an improved fuzzy comprehensive evaluation model, IFCE-α, based on the monitoring factor α, is proposed for evaluating the absorption window. Next, the radiative transfer simulation and inversion error analysis process for the absorption window was established based on the SCIATRAN model. Finally, the feasibility of the SCATF framework is verified by using atmospheric CO_2 as an illustrative example. Based on the experimental results, the SCATF framework demonstrates the ability to accurately extract the absorption characteristics of a specific gas, evaluate the extent of interference in both the absorption window and channel, and offer advanced insights into the performance of the absorption window in remote sensing detection. This framework introduces a novel approach for designing detection bands for atmospheric remote sensing.**

***Index Terms*—Fuzzy comprehensive evaluation, gas concentration inversion, HITRAN, radiative transfer, spectral characteristics analysis.**

I. Introduction

THE growing demand for atmospheric remote sensing has highlighted the need to extract, identify, and process absorption spectral characteristics of gases of interest. Precise identification of the "fingerprint" information in the gas absorption spectrum is crucial for quantifying the concentration or profile distribution of a target gas in remote sensing detection [1], [2]. However, extracting and quantitatively evaluating the absorption spectral characteristics of the target gas becomes challenging when multiple absorbing gases are present, despite the existing literature and relevant databases documenting most of the spectral features of molecules. Additional analysis and research are necessary to elucidate the methodological and technical aspects of gas absorption spectral characteristic extraction and analysis, as well as radiative transfer simulations [3], [4].

In recent decades, significant progress has been made in exploring and applying spectral features of molecules. Practical observations have revealed spectral features [5], [6], [7] of various molecules, including absorption line positions [8], [9], intensities [10], [11], and half-widths [12], [13]. The introduction of various simulation models [14], [15], [16], [17] has greatly enhanced the accuracy of simulated data related to spectral features. Moreover, several high-resolution molecular spectral databases, such as ExoMol [18], HITRAN/HITEMP [19], NIST [20], and PNNL [21] have been developed to compile spectral line data. The growing availability of spectral line information has fostered the development of hyperspectral imaging techniques based on molecular absorption spectroscopy [22]. Scholars involved in the development and design of gas sensors frequently utilize the extracted gas absorption spectral characteristics for designing inversion bands and conducting radiative transfer simulations [23], [24], [25] to gain insight into sensor performance beforehand.

Bridging spectral data and remote sensing applications involves several crucial steps, including spectral feature extraction and analysis, radiative transfer simulation, and technology validation. Several application program interfaces (APIs), such as HAPI [26], SpectraPlot [27], RADIS [28], and SPEARS [29], have been developed to enable more efficient extraction of molecular absorption spectra from spectral databases. These interfaces integrate a wide range of spectral line data, enabling researchers to accurately model absorption spectra across various wavelengths. However, interference or masking of the target

Manuscript received 4 June 2023; revised 13 September 2023; accepted 2 October 2023. Date of publication 6 October 2023; date of current version 23 October 2023. This work was supported in part by the National Major Scientific Instruments and Equipment Development Project of the National Natural Science Foundation of China under Grant 11727806 and in part by the General Program of the National Natural Science Foundation of China under Grant 41971283. *(Zhaocong Wu and Mingliang Li are co-first authors.) (Corresponding author: Mingliang Li.)*

Zhaocong Wu, Mingliang Li, Keyi Rao, and Yixian Yue are with the School of Remote Sensing and Information Engineering, Wuhan University, Wuhan 430079, China (e-mail: zcwoo@whu.edu.cn; lmliang@whu.edu.cn; kkkkae@whu.edu.cn; yueyixian@whu.edu.cn).

Anquan Xia is with the College of Resources and Environment, University of the Chinese Academy of Sciences, Beijing 100049, China (e-mail: xiaanquan17@mails.ucas.ac.cn).

Digital Object Identifier 10.1109/JSTARS.2023.3322640

gas absorption characteristics can occur when multiple gases absorb within the same absorption window, thereby reducing the availability of corresponding absorption channels. While the APIs have enhanced researchers' ability to retrieve molecular spectra, they still do not fully meet the need for quantitative analysis and evaluation of spectral properties.

This article aims to propose a method for quantitatively analyzing and evaluating spectral characteristics to enable the rapid quantitative analysis of absorption spectral characteristics of target gases in the presence of multiple interfering gases. Furthermore, a set of technical processes will be designed, ranging from molecular spectral databases to atmospheric remote sensing observation simulations. By doing so, a technical framework for the analysis of spectral characteristics for atmospheric remote sensing will be established. This framework not only accurately extracts the absorption characteristics of the target gas and quickly quantifies and evaluates the affected degree of absorption channels and absorption windows but also provides a preliminary analysis of the performance of absorption windows in remote sensing detection.

Fuzzy comprehensive evaluation models are more suitable for quantifying the extent to which the absorption spectral properties of gases are influenced. Various evaluation models are commonly used, including hierarchical process [30], a technique for order of preference by similarity to ideal solution method [31], data envelopment analysis [32], rank sum ratio method [33], fuzzy comprehensive evaluation [34], and gray relation analysis [35]. Using terms such as "large" or "small" to describe the degree of disturbance to an absorption characteristic is insufficient. The boundaries between good and bad absorption channels are not well defined, leading to a highly ambiguous concept. Hence, fuzzy comprehensive evaluation models are suitable for describing and studying this phenomenon.

HITRAN, a high-resolution spectral database, and SCIATRAN, a high-precision atmospheric radiative transfer model, serve as reliable data sources and analytical tools for studying absorption spectral characteristics. HITRAN contains 19 spectral parameters such as spectral line transition frequencies, spectral line intensities, and air broadening half-widths, which facilitate accurate modeling of the absorption spectra of gas molecules [36]. Atmospheric radiative transfer models such as MODTRAN [37], LBLRTM [38], and SCIATRAN [39] are extensively employed in remote sensing applications for precise modeling of solar radiation transfer in the atmosphere and at the surface. The SCIATRAN model, which integrates various cloud, aerosol, and surface parameterization methods, has adjustable parameters and high computational accuracy, making it a highly promising tool for gas detection simulation.

This article proposes an improved fuzzy comprehensive evaluation (IFCE) method for the analysis of the influence degree of gas absorption spectrum characteristics and constructs a technical framework, called spectrum characteristics analysis technical framework (SCATF), concerning atmospheric remote sensing. Initially, the molecular absorption spectra are simulated using the HITRAN database, and the method for extracting absorption windows is investigated. Subsequently, a fuzzy membership function is designed, and the fuzzy comprehensive evaluation model is improved to facilitate the evaluation of absorption channels. Based on this, the IFCE-α model, an IFCE model incorporating the monitoring factor α, is proposed for assessing absorption windows. Finally, sensitivity analysis and inversion are performed using the SCIATRAN model to analyze the performance of absorption windows in remote sensing detection.

II. Methodology

To achieve the proposed objectives of this study, three critical issues need to be addressed. The first issue involves extracting the effective absorption characteristics of the target gas. The second problem revolves around establishing an evaluation model to accurately quantify the absorption characteristics of the target gas. Finally, the third challenge relates to conducting remote sensing detection simulations for the absorption window. To address the first problem, we utilize the HITRAN database along with the threshold method to extract absorption bands. For the second challenge, we propose an IFCE-α model that incorporates the monitoring factor α. The third issue is effectively addressed by reasonably establishing observation scenarios, employing sensitivity analysis techniques, and utilizing optimal inversion algorithms.

Fig. 1 illustrates the fundamental components and functions of the SCATF framework developed in this article. The framework consists of three parts: absorption spectrum simulation and extraction of absorption windows, improvement of fuzzy comprehensive evaluation model and evaluation of absorption windows, and absorption window radiative transfer simulation. The processes involved in each part are explained as follows.

1) Based on the high-resolution molecular spectral library, the absorption spectra of the target gas and other atmospheric gas components are simulated across the entire spectral range. Subsequently, according to the absorption intensity of the target gas, the absorption spectra of the target gas and other gases are extracted using the threshold method.
2) According to the absorption spectrum characteristics, a membership function is constructed. Subsequently, by replacing the fuzzy operator, an IFCE model is established to evaluate the affected degree of the absorption channel of the target gas. Furthermore, by introducing the monitoring factor α, an IFCE-α model is built to evaluate the affected degree of the absorption window of the target gas.
3) Satellite observation scenarios are established based on simulation requirements. Next, the radiance sensitivity and signal-to-noise ratio (SNR) requirements are analyzed by using the SCIATRAN model. In addition, the column averaging kernel and a posteriori inversion error is derived based on the optimal inversion algorithm. Finally, the performance of the absorption window in remote sensing detection is analyzed.

A. Absorption Window Extraction

The HITRAN2020 database[1] enables researchers to compute absorption spectra for different atmospheric gases within the

[1] [Online]. Available: https://hitran.iao.ru

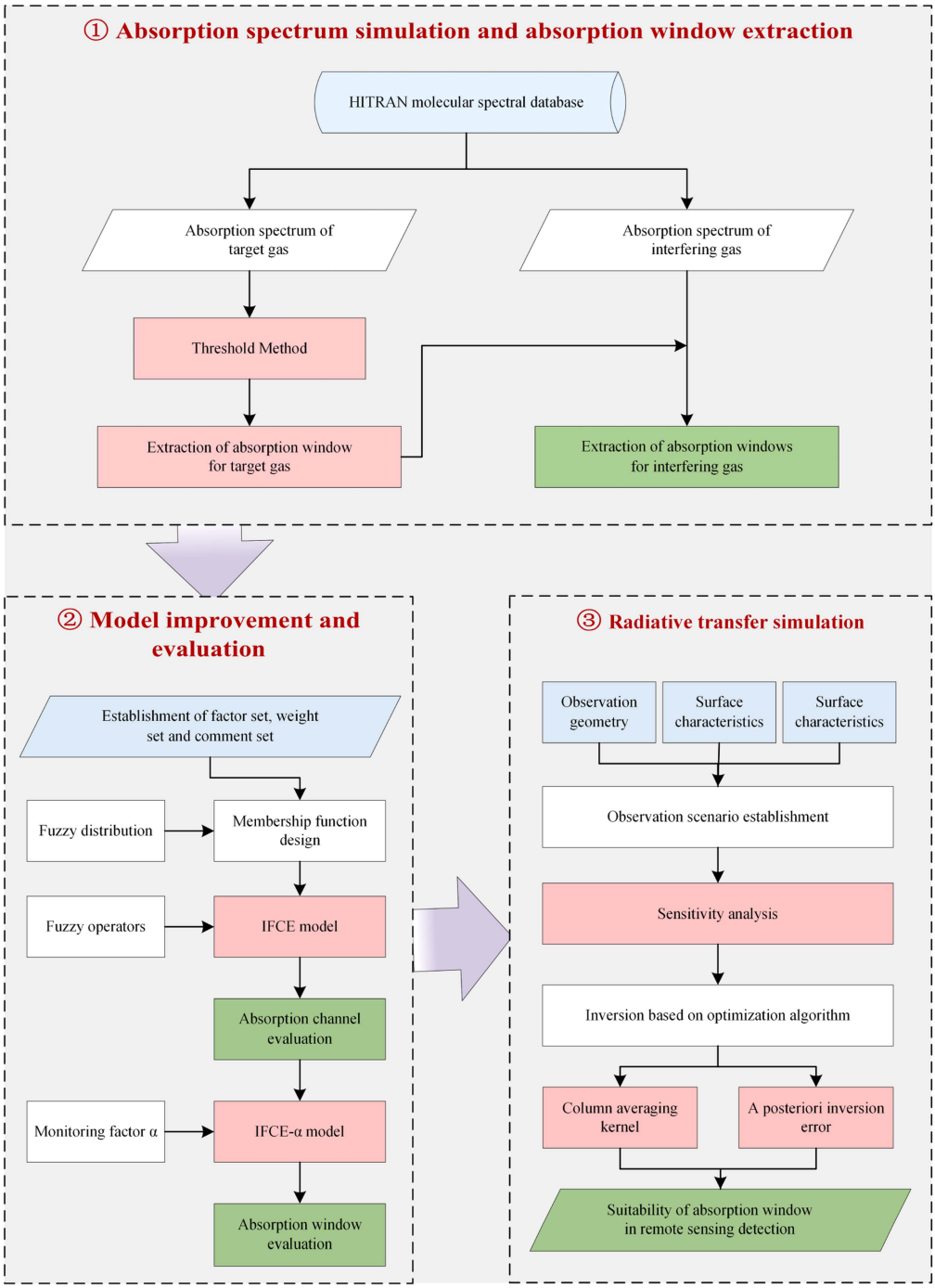

Fig. 1. SCATF framework for atmospheric remote sensing detection.

effective spectral range documented in HITRAN. The specific spectral range can be tailored according to specific requirements.

The gas absorbance function [40] can be expressed as follows:

$$AF(WN,T,P,L) = 1 - e^{-KN_a(WN,T,P)L} = 1 - e^{-KN_a(WN,T,P)CL'} \quad (1)$$

where AF is the gas absorbance function (Absorption rate), KN_a is the molecular absorption coefficient per unit volume of pure gas molecules, WN is the current wave number (cm^{-1}), T represents the temperature (K), P denotes the pressure (hPa), and L is the radiative transfer path of pure gas, referred to as the relative radiative transfer path in this article. C is the gas concentration and L' is the radiative transfer path in the actual satellite observation.

Considering that most atmospheric molecules are concentrated within a 10 000 m range from the Earth's surface, this study defines the actual radiation transfer path, denoted as L', as 10 000 m. Consequently, a magnification factor of 10 000 is applied to the concentration of molecules in the atmosphere to

determine the relative radiative transfer path L. This approach effectively eliminates the errors that caused by the abnormal number of molecules along the optical path.

Analyzing absorption characteristics within specific absorption windows, which comprise particular absorption channels, is a common approach to meet the requirements of diverse remote sensing applications. Hence, the effective extraction of these absorption windows is crucial as a prerequisite. In this study, absorption rate thresholds and bandwidth thresholds are employed to achieve this objective.

At the beginning, the absorption threshold is used to divide the absorption spectrum into segments. Due to electronic transitions, molecular vibrations, and rotations, pollutants such as NO_X, SO_2, CO_2, and CH_4 exhibit distinct band-shaped absorption spectra at high spectral resolutions. In addition, the absorption rate is nearly negligible in weak absorption channels and nonabsorbing bands. To divide the absorption spectrum into segments using the threshold method, it is essential to determine an appropriate threshold value based on the specific application. In the context of atmospheric remote sensing, the energy changes caused by an extremely low gas absorption rate are insignificant. As a result, this study sets the threshold value for the absorption rate to 10^{-10}, considering absorption coefficients below this threshold as zero. This approach facilitates the extraction of the desired gas absorption window, providing valuable information regarding the location and intensity of each window. To achieve a more precise assessment of the impact of the absorption window, it may be necessary to manually adjust the window's span to a minimum while preserving the integrity of the gas absorption band.

The second step involves applying the bandwidth threshold to remove absorption windows that are considered invalid for remote sensing detection. A narrow absorption window is usually unusable and, thus, classified as invalid. The width threshold of the window depends on the gas type and the window's position. The total carbon column observation network [41], [42] has continuously observed gases such as CO_2, CH_4, CO, N_2O, and others for an extended period using a spectrometer with a detection bandwidth greater than 20 cm^{-1}. To retain more effective bands for a detailed analysis, this study sets a window width threshold of 15 cm^{-1} and excludes windows with a width smaller than this threshold during the extraction process.

Finally, the absorption spectra of other atmospheric gas molecules are acquired based on the absorption windows of the target gas in order to evaluate their influence on the absorption spectrum of the target gas.

The present study employed the threshold method to extract N_2O absorption windows in order to evaluate its effectiveness. The results indicated that 52 absorption windows were obtained using absorbance thresholds, and after applying window threshold filtering, 49 windows were extracted. The extracted windows encompassed those employed for the remote sensing inversion of N_2O concentration [43], [44], such as 1240–1350 cm^{-1}, 2130–2280 cm^{-1}, 4300–4450 cm^{-1}, and 4665–4785 cm^{-1}. These findings suggest the effectiveness of the threshold method in the band selection process. Fig. 2 illustrates a section of the N_2O absorption window extracted using the threshold method.

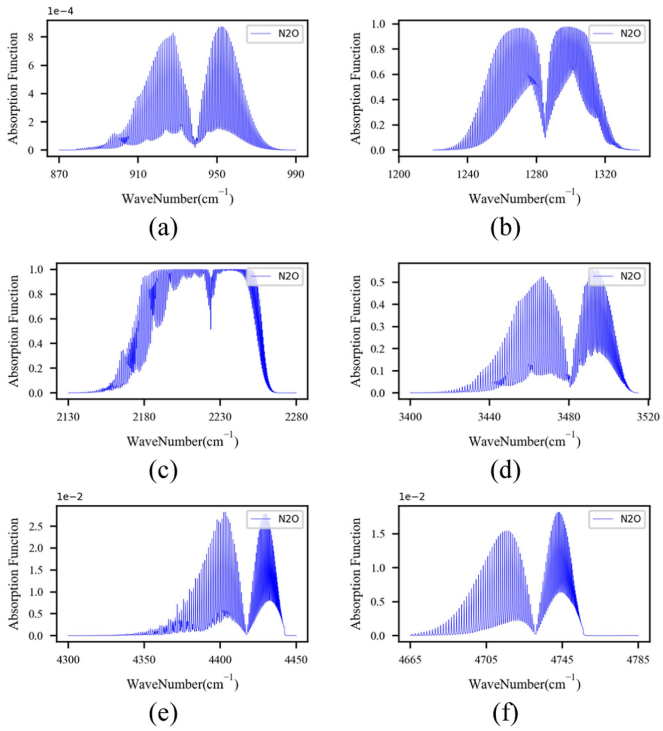

Fig. 2. N_2O absorption window extracted using the threshold method.

B. Establishment of Factor Set, Weight Set, and Comment Set

To provide a clear and explicit demonstration of the establishment process of the fuzzy membership function, this article initially defines the evaluation indexes, index weights, and evaluation results, referred to as the factor set, weight set, and comment set.

In this study, the absorption channel and absorption window are employed as the units of analysis. Consequently, the absorption spectrum of the target gas within its absorption window can be represented as A_{i0}

$$A_{i0} = [a_{i0}(\lambda_1),\ a_{i0}(\lambda_2), \ldots, a_{i0}(\lambda_k), \ldots,\ a_{i0}(\lambda_{p_i})] \quad (2)$$

where the subscript i denotes the index of the absorption window ($i = 1, 2, \ldots, m$), the subscript *0* denotes the target gas, $a_{i0}(\lambda_k)$ denotes the absorption coefficient of channel λ_k ($k = 1, 2, \ldots, p_i$), and p_i denotes the number of absorption channels within the *i*th absorption window.

Taking into account the existence of multiple interfering gases within the absorption window of the target gas, the absorption spectrum of these interfering gases can be expressed as A_{ij}

$$A_{ij} = [a_{ij}(\lambda_1),\ a_{ij}(\lambda_2), \ldots, a_{ij}(\lambda_k), \ldots,\ a_{ij}(\lambda_{p_i})] \quad (3)$$

where the subscript i denotes the index of the absorption window ($i = 1, 2, \ldots, m$), the subscript j represents the interfering gas species ($i = 1, 2, \ldots, n$), and $a_{ij}(\lambda_k)$ denotes the absorption coefficient of the *j*th interfering gas in channel λ_k ($k = 1, 2, \ldots, p_i$).

To better understand the influence of a gas on the absorption characteristics of the target gas, we define the factor set as the ratio between the absorption coefficient of the interfering gas and

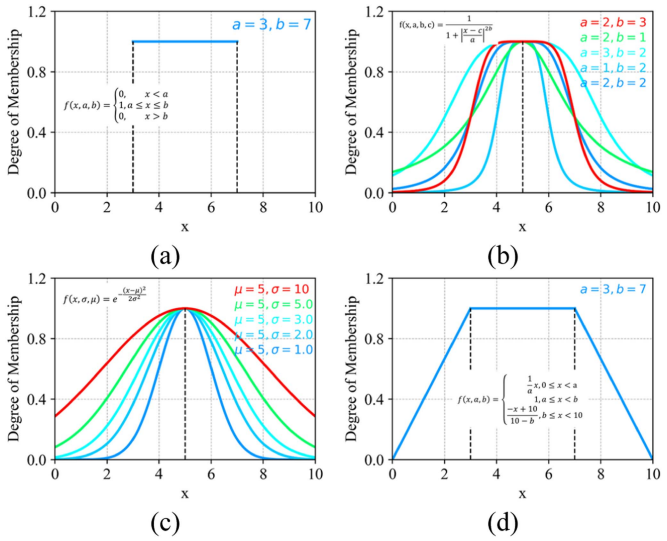

Fig. 3. Visualization of fuzzy distributions. (a) Rectangular. (b) Generalized bell-shaped. (c) Gaussian. (d) Trapezoidal distributions.

that of the target gas. A higher ratio signifies a stronger absorption characteristic of the interfering gas, which can overshadow the absorption characteristic of the target gas. Conversely, a lower ratio indicates the dominance of the absorption characteristics of the target gas. The factor set U_i can be mathematically expressed as

$$U_i\ (\lambda_k) = \{u_{i1}\,(\lambda_k), u_{i2}\,(\lambda_k), \ldots, u_{ij}\,(\lambda_k), \ldots, u_{in}\,(\lambda_k)\} \tag{4}$$

where $u_{ij}\,(\lambda_k) = a_{ij}\,(\lambda_k)/a_{i0}(\lambda_k)$ is the ratio of the absorption coefficient of the *j*th interfering gas to that of the target gas.

The absorption characteristics of the target gas are influenced by the absorption coefficient of the interfering gas, irrespective of the gas type. Therefore, it is reasonable to assign equal weights to the weight set *W* when evaluating the impact on individual channels of the target gas: $W = \{w_j, w_j = 1/n\}$.

To describe the level of impact on a channel within the absorption window of the target gas, four affected levels are defined, i.e., the comment set $\mathrm{V} = \{1-\text{unaffected}, 2-\text{slightly affected}, 3-\text{greatly affected}, 4-\text{seriously affected}\}$.

C. Construction of Fuzzy Membership Function

This article argues that the trapezoidal or semitrapezoidal distribution is the optimal choice for constructing the fuzzy membership function. Although there are various fuzzy distributions available, such as rectangular, Gaussian, and bell-shaped distributions, not all of them are suitable for our study. As Fig. 3 illustrates, rectangular or semirectangular distributions are overly simplistic, primarily aimed at conveying deterministic information and they do not effectively capture the fuzziness associated with the absorbed characteristic interference. The functional form of the generalized bell-shaped distribution is more intricate, rendering parameter determination more challenging and amplifying the uncertainty in experimental outcomes. The membership degree of the Gaussian distribution equals 1 only at the center point (mean) of the curve. This indicates that the Gaussian distribution is excessively conservative in conveying deterministic information and does not meet the prerequisites of this study. In contrast, the trapezoidal or semitrapezoidal distribution function exhibits a straightforward structure and explicit parameter interpretations. It simultaneously addresses both information determinacy and fuzziness, aligning with the criteria of this article.

The membership functions, constructed based on the trapezoidal or semitrapezoidal distribution, are represented by (5)–(8).

For independent variable values below 0.01, the membership value of the membership function $r^1(x)$ is 1. This suggests that the absorption characteristics of the target gas remain unaffected. However, as the independent variable increases within the range of 0.01–0.02, the membership value decreases. The specific value can be determined using the corresponding segment within the piecewise function. For independent variable values greater than 0.02, the membership value is 0. This indicates that the absorption characteristics of the target gas are no longer at the "unaffected" level. The first two segments are defined with a width of 0.01, and the narrower range of values considers the uncertainty in the degree of affected absorption characteristics while preserving deterministic information.

The function $r^2(x)$ indicates that for independent variable values less than 0.01, the target gas absorption characteristics do not fall under the category of "slightly affected" and align with the findings from $r^1(x)$. However, as the independent variable falls within the range of 0.01–0.02, the membership degree increases proportionally. In contrast, for independent variable values between 0.02 and 0.5, the membership degree decreases as the independent variable increases until the target gas absorption characteristics are no longer considered "slightly affected." When the independent variable falls within the range of 0.02–0.2, the membership degree is 1, indicating that the target gas absorption characteristics are entirely classified as "slightly affected."

$$r^1\ (x) = \begin{cases} 1, & 0 \le x < \frac{1}{100} \\ -100x + 2, & \frac{1}{100} \le x < \frac{1}{50} \\ 0, & x \ge \frac{1}{50} \end{cases} \tag{5}$$

$$r^2\ (x) = \begin{cases} 0, & 0 \le x < \frac{1}{100} \\ 100x - 1, & \frac{1}{100} \le x < \frac{1}{50} \\ 1, & \frac{1}{50} \le x < \frac{1}{5} \\ -\frac{10}{3}x + \frac{5}{3}, & \frac{1}{5} \le x < \frac{1}{2} \\ 0, & x \ge \frac{1}{2} \end{cases} \tag{6}$$

$$r^3\ (x) = \begin{cases} 0, & 0 \le x < \frac{1}{5} \\ \frac{10}{3}x - \frac{2}{3}, & \frac{1}{5} \le x < \frac{1}{2} \\ 1, & \frac{1}{2} \le x < 2 \\ -\frac{1}{3}x + \frac{5}{3}, & 2 \le x < 5 \\ 0, & x \ge 5 \end{cases} \tag{7}$$

$$r^4\ (x) = \begin{cases} 0, & 0 \le x < 2 \\ \frac{1}{3}x - \frac{2}{3}, & 2 \le x < 5 \\ 1, & x \ge 5 \end{cases}. \tag{8}$$

In (5)–(8), x represents the evaluation indicator, i.e., the element in factor set U_i.

The interpretations attributed to the cut-off points of the $r^3(x)$ and $r^4(x)$ functions are analogous to those of the $r^1(x)$ and $r^2(x)$ functions, hence they shall not be reiterated herein.

Thus, the membership matrix $R_{ij}(\lambda_k)$ for a single evaluation indicator $u_{ij}(\lambda_k)$ can be expressed as follows:

$$R_{ij}\ (\lambda_k) = \left[r_{ij}^1\ (\lambda_k), r_{ij}^2\ (\lambda_k), r_{ij}^3\ (\lambda_k), r_{ij}^4\ (\lambda_k)\right]. \tag{9}$$

The expression of the fuzzy comprehensive evaluation matrix $R_i(\lambda_k)$ is as follows:

$$R_i\ (\lambda_k) = [R_{i1}\ (\lambda_k), R_{i2}\ (\lambda_k), \ldots, R_{ij}\ (\lambda_k), \ldots, R_{in}\ (\lambda_k)]^T. \tag{10}$$

D. Absorption Channel Evaluation Method IFCE

The conventional fuzzy comprehensive evaluation model, as shown in (11), employs classical fuzzy operators [such as $M(\vee, \wedge)$, $M(\vee, \cdot)$, $M(\oplus, \wedge)$, and$M(+, \cdot)$] to combine the information from the fuzzy comprehensive evaluation matrix R and calculate the fuzzy evaluation vector B. Consequently, the evaluation results are obtained by following the maximum membership principle

$$B_i\ (\lambda_k) = W \circ R_i\ (\lambda_k). \tag{11}$$

In the assessment of absorption channels, the classical fuzzy operator may weaken and lose valuable information. As a result, accurate evaluation results are often not achieved. To address this issue, a modification of the classical fuzzy operator has been proposed. This modified approach utilizes level variables and the "max" operator to enhance the evaluation process. Specifically, the level variables are employed to weigh the membership degrees in the evaluation matrix R, thus maximizing the use of available information. The "max" operator is then applied to highlight the weighted results, leading to more accurate evaluation outcomes. The IFCE model is presented as follows:

$$H_{ij}\ (\lambda_k) = \sum_{q=1}^{4} v_q \cdot r_{ij}^q\ (\lambda_k) \tag{12}$$

$$H_i\ (\lambda_k) = \bigvee_j H_{ij}\ (\lambda_k) \tag{13}$$

where $H_{ij}(\lambda_k)$ is the level-variable-weighted value (LVW), and v_q corresponds to numerical representations of elements in the comment set V. $H_i(\lambda_k)$ denotes the maximum LVW value among n gases in channel λ_k, with $H_i(\lambda_k) \subseteq [1, 4]$, indicating a range from 1 to 4. $\vee$ is the "max" operator.

For example, if channel λ_0 of the target gas GAS_X is affected by five interfering gases, the fuzzy comprehensive evaluation matrix $R(\lambda_0)$ obtained based on the fuzzy membership function is

$$R\ (\lambda_0) = (r_{jq})_{5\times 4} = \begin{bmatrix} 0 & 0 & 0 & 1 \\ 0.3 & 0.7 & 0 & 0 \\ 1 & 0 & 0 & 0 \\ 0.8 & 0.2 & 0 & 0 \\ 0.5 & 0.5 & 0 & 0 \end{bmatrix}$$

where r_{jq} represents the membership degree of the jth factor to the qth comment; $j = 1, 2, \ldots, 5$ representing the type of interfering gas; $q = 1, 2, \ldots, 4$ representing four comments described in Section II-A1.

According to the principle of maximum membership degree, r_{14} is equal to 1, indicating that the first gas causes channel λ_0 to be seriously affected. Similarly, r_{22} is 0.7, r_{31} is 1, and r_{41} is 0.8, suggesting that the second gas causes channel λ_0 to be greatly affected, whereas the third and fourth gases do not have any effect on channel λ_0. The exact effect of the fifth gas cannot be determined as r_{51} and r_{52} are both 0.5. For an absorption channel, the severity of the final result will not be mitigated even if only one gas has a severe effect on it. Therefore, the absorption characteristics of the target gas on this channel will be difficult to identify in the presence of five gas interferences.

The influence level of channel λ_0 was assessed using the conventional fuzzy comprehensive evaluation model. The evaluation yielded a fuzzy evaluation vector B of [0.8, 0.6, 0, 0.2]. The membership degree for the "unaffected" level was determined to be 0.8, which contradicts the actual situation. However, upon recalculation using IFCE, the LVW of the five evaluation indicators for channel λ_0 was determined as $H_{ij}\ (\lambda_0) = [4, 1.7, 1, 1.2, 1.5]$, with a maximum LVW of $H_i\ (\lambda_0) = 4$. This indicates that the channel is significantly affected. The accuracy of the IFCE evaluation results is evident.

E. Absorption Window Evaluation Method IFCE-α

The affected degree of the absorption window is evaluated by synthesizing the maximum LVW values $H_i(\lambda_k)$ of all channels and obtaining the LVW corresponding to the window, denoted as H_i. In the absorption window of the target gas, the channel located at the center of the absorption line exhibits significant radiation absorption, referred to as the "strong absorption channel." Conversely, the channels positioned at the edges demonstrate relatively weak absorption of radiation, referred to as the "weak absorption channels." Thus, the evaluation result of the absorption window relies on how the strong and weak absorption channels within the window are processed.

If $H_i(\lambda_k)$ is averaged over all channels, the improved fuzzy comprehensive evaluation model based on the mean-value method (IFCE-M) can be obtained

$$\begin{aligned} H_i &= \frac{1}{p_i}\sum_{k=1}^{p_i} H_i(\lambda_k) \\ &= \frac{1}{p_i^{\text{peak}} + p_i^{\text{val}}}\sum_{k=1}^{p_i^{\text{peak}}} H_i(\lambda_k^{\text{peak}}) + \frac{1}{p_i^{\text{peak}} + p_i^{\text{val}}}\sum_{k=1}^{p_i^{\text{val}}} H_i(\lambda_k^{\text{val}}) \end{aligned} \tag{14}$$

where λ_k^{peak} and λ_k^{val} represent the strong absorption channels and the weak absorption channels, respectively. p_i^{peak} and p_i^{val} are the numbers of strong absorption channels and weak absorption channels, respectively.

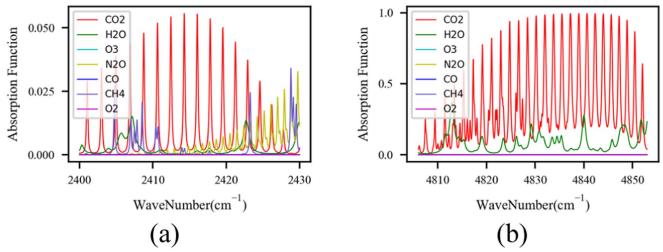

Fig. 4. Example windows with spectral ranges of (a) 2400–2430 cm^{-1} and (b) 4806–4853 cm^{-1}, spectral resolution of 0.01 cm^{-1}, target gas as CO_2, and six interfering gases as H_2O, O_3, N_2O, CO, CH_4, and O_2.

TABLE I
EVALUATION RESULTS OF ABSORPTION WINDOWS (A) AND WINDOWS (B)

Window	Truth	IFCE-M	IFCE-α (α = 0.5)
(a)	slightly affected	$H_a = 2.91$ greatly affected	$H_a = 2.36$ slightly affected
(b)	slightly affected	$H_b = 2.40$ slightly affected	$H_b = 2.29$ slightly affected

The affected level of the absorption window can be expressed as follows:

$$S_i = \begin{cases} \text{unaffected}, & [H_i] = 1 \\ \text{slightly affected}, & [H_i] = 2 \\ \text{greatly affected}, & [H_i] = 3 \\ \text{seriously affected}, & [H_i] = 4 \end{cases} \tag{15}$$

where the symbol [] represents rounding. "Slightly affected" indicates that the absorption characteristics in the window experience minimal impact and do not impede its usability. "Greatly affected" suggests significant limitations to the usability of the window. "Seriously affected" indicates that the absorption characteristics of the target gas within the absorption window are nearly indistinguishable.

To assess the performance of the mean value method (or IFCE-M) in evaluating absorption windows, two windows were selected as examples: 2400–2430 cm^{-1} [referred to as window (a)] and 4806–4853 cm^{-1} [referred to as window (b)]. These windows were analyzed to determine the impact of the six interfering gases on the CO_2 absorption characteristics within them.

According to Fig. 4, Window (a) is affected by CH_4, N_2O, and H_2O, while window (b) is mainly impacted by H_2O. Visual analysis may indicate that window (a) is more affected than window (b); however, this is not always the case. Although window (a) has more interfering gases with higher absorption coefficients, their absorption lines seldom coincide with CO_2 absorption lines, leading to minimal impact on the CO_2 absorption characteristics.

According to Table I, the IFCE-M evaluation results for window (b) align with the actual observations, whereas those for window (a) do not show the same consistency. This phenomenon can be attributed to the following reasons: when the strong absorption channel of the interfering gas roughly aligns with the strong absorption channel of the target gas, it has a significant impact on the absorption characteristics of the target gas; conversely, when the strong absorption channel of the interfering gas is close to the weak absorption channel of the target gas, the influence on the absorption characteristics of the target gas is relatively minimal. Apparently, the IFCE-M method does not consider the differences between strong and weak absorption channels, making it somewhat inadequate for assessing window levels.

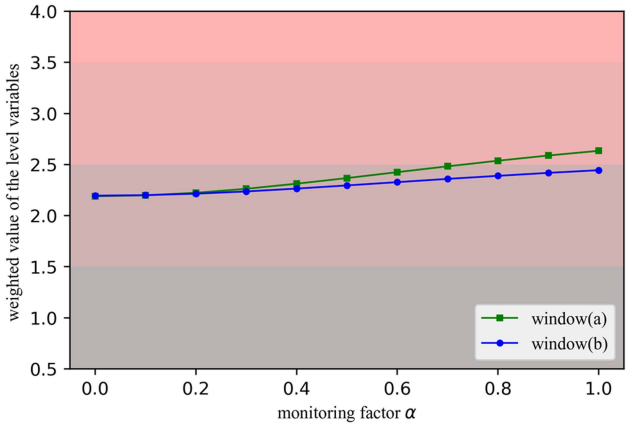

Fig. 5. Correspondence between the monitoring factor α and LVWs for windows (a) and (b).

To address the limitations of IFCE-M, this article presents an enhanced fuzzy comprehensive evaluation model called IFCE-α. The proposed model incorporates a monitoring factor α ($\alpha \subseteq [0, 1]$) in the calculation of H_i ($H_i \subseteq [0.5, 4]$). The monitoring factor α is introduced to emphasize the difference between strong and weak absorption channels of the target gas during the evaluation process.

$$H_i = \frac{1}{1+\alpha^2}\left[\frac{1}{p_i^{\text{peak}}}\sum_{k=1}^{p_i^{\text{peak}}} H_i(\lambda_k^{\text{peak}}) + \alpha^2 \frac{1}{p_i^{\text{val}}}\sum_{k=1}^{p_i^{\text{val}}} H_i(\lambda_k^{\text{val}})\right]. \tag{16}$$

Equation (16) demonstrates that the window evaluation is exclusively determined by the strong absorption channels when $\alpha = 0$, disregarding the weak absorption channels. Conversely, when $\alpha = 1$, both the strong and weak absorption channels are given equal consideration. The value of the monitoring factor α can be determined empirically or obtained through feedback on the evaluation results.

Based on Table I, the IFCE-α model accurately evaluates both window (a) and window (b). The LVWs for the two absorption windows are 2.36 and 2.29 when α is 0.5, respectively. These values correspond to "slightly affected," aligning with the actual situation.

This article also investigates the stability of the IFCE-α model. According to Fig. 5, as α changes from 1 to 0, the LVW for window (b) ranges from 2.19 to 2.44, indicating a "slight effect." The LVW in window (a) gradually changes from 2.64 to

TABLE II
OBSERVATION SCENARIO PARAMETERS

Parameter Type	Parameter
spectral parameters	band
	Spectral resolution
observation geometry	Solar zenith angle
	Observation mode
	Sensor altitude
atmospheric state	Atmospheric profile
	Aerosol type
	AOD
surface characteristics	Surface type
	albedo

2.18, indicating a transition from "largely affected" to "slightly affected" and correcting the initially incorrect evaluation result. The LVWs exhibit gradual changes without significant fluctuations, providing robust evidence for the stability of the IFCE-α model.

F. Observation Scenario Establishment

The establishment of a well-defined observation scenario is crucial for the successful implementation of radiative transfer simulation. Key factors in establishing an observation scenario include determining crucial parameters, such as spectral characteristics, observation geometry, atmospheric conditions, and surface properties, as outlined in Table II.

The selection of band and spectral resolution should be based on the specific remote sensing detection requirements and can be optimized based on the simulation results.

The observation geometry can be determined using a mathematical model. The following equation describes the temporal, seasonal, and latitudinal variations of the solar zenith angle (SZA):

$$\sin\left(\frac{\pi}{2}-\theta_s\right)=\cos h\ \cos\delta\cos\Phi+\sin\delta\sin\Phi \tag{17}$$

where θ_s is the SZA, h is the solar hour angle, δ is the current solar declination, and Φ is the local latitude.

Atmospheric state parameters and surface characteristic parameters can be retrieved from widely accessible databases. When referring to atmospheric profiles, researchers can choose from the 1976 American Standard Atmosphere [45] or the European TIGR [46] atmospheric profile database, both of which provide atmospheric models for tropical, midlatitude, and polar regions. Options for aerosol types include MODIS, AERONET [47], and Optical Properties of Aerosols and Clouds [48], which can generate a wide range of aerosol types by combining basic aerosol particles. The aerosol optical depth (AOD) can be determined based on the desired accuracy requirements for target gas detection, such as specifying the limit value, median value, or a series of equally spaced values of AOD.

Simplifying the surface model as a Lambertian body is a common practice in radiative transfer simulations. This approach allows for the extraction of surface reflectance values from a range of spectral databases, such as the ASTER spectral library [49] and the USGS digital spectral library [50]. When dealing with a narrow band, assuming a constant surface reflectance is also acceptable.

G. Sensitivity Analysis and Inversion

It is important to note that in the strong absorption window, radiation absorption can easily saturate, posing challenges to the accurate detection of target gas concentrations. Conversely, in the weak absorption window, variations in target gas concentration may cause minimal radiance fluctuations, resulting in reduced sensitivity and hindering gas detection efforts. Therefore, conducting remote sensing simulations of the absorption window is crucial to assess its performance in remote sensing detection.

The radiative transfer process under real atmospheric conditions can be described as follows:

$$R\ =\ F\left(x\right)+\varepsilon \tag{18}$$

where R is the radiance received by the sensor, F is the forward radiative transfer model, x denotes the state parameter to be inverted, and ε represents the model and observation errors.

When considering a specific absorption window, the initial step is to examine the sensitivity of the radiance to changes in the target gas concentration. This sensitivity analysis is crucial in determining whether the absorption window is suitable for remote sensing detection of the target gas. In addition, it is crucial to investigate other factors, including spectral resolution, SZA, aerosol type, AOD, and surface reflectance, as these variables significantly influence the accuracy of the remote sensing detection of target gases.

The radiance sensitivity is quantified by the relative rate of change of radiance, which can be defined as follows:

$$S=\frac{\Delta R}{R_0}=\frac{R'-R_0}{R_0} \tag{19}$$

where S represents the sensitivity, R_0 is the radiance under the initial scenario, and R' is the radiance after the observed scenario parameters are changed. The SNR is defined as the reciprocal of radiance sensitivity.

The optimal inversion algorithm [51] is employed to obtain the maximum likelihood solution of the model by minimizing the following cost function:

$$\begin{aligned}\chi^2=&\left[R-F(x)\right]^T S_\varepsilon^{-1}\left[R-F(x)\right]\\&+\gamma(x-x_a)^T S_a^{-1}(x-x_a)\end{aligned} \tag{20}$$

where S_ε is the measurement error covariance matrix, S_a is the a priori covariance matrix, and x_a is an a priori state vector.

The Levenberg–Marquardt iterative method is employed to accelerate the convergence speed during the solution process as follows:

$$\begin{aligned}x_{i+1}=x_0\ &+\left(K_i^T S_\varepsilon^{-1}K_i+\gamma S_a^{-1}\right)^{-1}\\&\times\left[K_i^T S_\varepsilon^{-1}\left(R-F\left(x_i\right)\right)+S_a^{-1}\left(x_i-x_0\right)\right]\end{aligned} \tag{21}$$

TABLE III
GAS SPECIES, CONCENTRATIONS, AND SIMULATION BANDS

Gas species	wavenumber range (cm^{-1})	Concentration (%)
CH_4	0–11 500	0.00017
CO	4–14 477	0.000015
CO_2	158–19 908	0.033
H_2O	0–42 000	1.86
N_2O	0–7796	0.000032
O_2	0–57 027	20.9
O_3	0–6996	0.000003

where subscript i represents the number of iterations, $K = \partial F(x)/\partial x$ is the Jacobi matrix, and γ represents the Levenberg–Marquardt parameter, which is initialized to 1.

In this study, the inversion error is quantified using the standard deviation, and the sensitivity of gas inversion at different altitudes is assessed using the column averaging kernel. A smaller column averaging kernel at a specific height indicates a lower sensitivity of gas inversion at that height. In ideal cases, the elements of the column averaging kernel are equal to 1, indicating a perfect match between the gas profile obtained by the inversion and the true profile. The posterior error covariance matrix and the averaging kernel can be calculated as follows:

$$\hat{S} = \left(K^T S_\varepsilon^{-1} K + S_a^{-1}\right)^{-1} \tag{22}$$

$$\mathrm{A} = \frac{\partial \hat{x}}{\partial x} = \hat{S}\, K^T S_\varepsilon^{-1} K. \tag{23}$$

The standard deviation of the error in inversion values σ_{XCO2} is given as follows:

$$\sigma_{\mathrm{XCO2}} = \left(h^T \hat{S} h\right)^{1/2} \tag{24}$$

where h represents the pressure weighting function [52].

The column averaging kernel for layer j can be calculated as follows:

$$a_j = \left(h^T A\right)_j \frac{1}{h_j}. \tag{25}$$

So far, the technical framework for atmospheric remote sensing, SCATF, has been successfully established through the application of the absorption window extraction method, spectral characteristic analysis method, and absorption window remote sensing simulation method.

III. CASE STUDY

This study examines the SCATF framework by using atmospheric CO_2 as a case study. We specifically analyze how six atmospheric gases (see Table III) with pronounced absorption properties, which are of significant concern in air pollution, affect the CO_2 absorption spectral characteristics. In addition, we investigate the initial feasibility of employing the chosen CO_2 absorption window for atmospheric remote sensing detection across different observation scenarios.

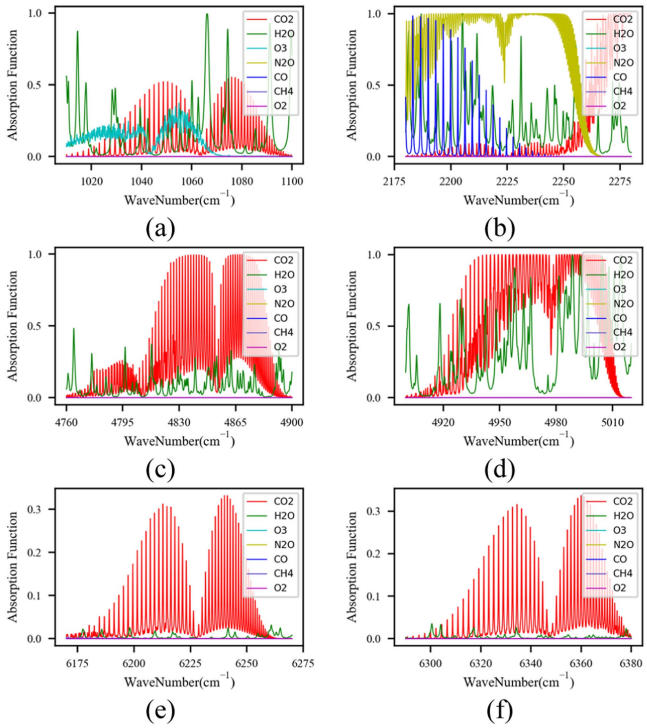

Fig. 6. Absorption spectra of seven gases within the CO_2 absorption window.

A. Absorption Window Extraction Results

The threshold method was used to extract 60 absorption windows for CO_2 according to its absorption coefficient. These extracted absorption windows were then utilized to simultaneously extract the absorption spectra of the remaining six gases within the same windows. Fig. 6 shows some representative CO_2 absorption windows, and all absorption windows are given in Appendix A.

The CO_2 absorption characteristics in the six windows, as illustrated in Fig. 6, are clearly evident, and nearly all of them are affected by water vapor. Notably, windows (a), (c), and (d) exhibit numerous moderate-intensity water vapor absorption lines, which are the main influencing factors of the CO_2 absorption characteristics. Furthermore, window (a) is also affected by a prominent vibrational rotational spectral band of O_3. Window (b) experiences significant interference from H_2O, CO, and N_2O simultaneously. In contrast to the remaining four windows, windows (e) and (f) exhibit a minor presence of weak absorption lines associated with water vapor, resulting in lower levels of interference. The degree of interference positively correlates with the water vapor content.

To facilitate the assessment of the accuracy of the IFCE-α evaluation results, the affected degree of absorption windows was determined in advance using an expert scoring method [53] in this article, and the results are given in Table IV. Out of the 60 absorption windows, 2 were unaffected, 2 were slightly affected, 13 were greatly affected, and the remaining 43 were greatly affected. The results of expert scoring were used as a reference to verify the evaluation results of IFCE-α.

TABLE IV
EVALUATION RESULTS OF CO_2 ABSORPTION WINDOW

Absorption windows (cm^{-1})	Expert scoring	IFCE-α	Absorption windows (cm^{-1})	expert scoring	IFCE-α
290 – 362	4	4	6020 – 6120	3	3
500 – 542	4	4	6170 – 6270	1	2
550 – 630	3	3	6290 – 6380	1	2
710 – 790	3	3	6450 – 6570	3	3
795 – 835	4	4	6890 – 6990	4	4
915 – 1000	3	3	7174 – 7220	4	4
1010 – 1100	4	3	7220 – 7330	4	4
1136 – 1165	4	4	7410 – 7500	4	4
1166 – 1191	4	4	7520 – 7630	4	4
1572 – 1590	4	4	7680 – 7790	4	4
1596 – 1618	4	4	7863 – 7990	4	4
1687 – 1750	4	4	8130 – 8210	4	4
1753 – 1779	4	4	8220 – 8310	4	4
1880 – 1940	4	4	8632 – 8712	4	4
2020 – 2135	4	3	8769 – 8873	4	4
2180 – 2280	3	3	8910 – 8999	4	4
2400 – 2460	3	3	9100 –9168	4	4
2973 – 3032	4	4	9330 – 9410	4	4
3240 – 3400	4	4	9430 – 9535	3	3
3480 – 3590	3	3	9546 – 9652	4	4
3640 – 3690	3	3	10 174 – 10 188	4	4
3740 – 3850	3	3	10 198 – 10 213	4	4
4319 – 4344	4	4	10 540 – 10 564	4	4
4347 – 4476	4	4	10 569 – 10 587	4	4
4760 – 4900	2	2	10 662 – 10 744	4	4
4900 – 5020	2	3	10 778 – 10 860	4	4
5040 – 5160	3	3	10 949 – 11 007	4	4
5472 – 5600	4	4	11 430 – 11 508	3	3
5610 – 5705	4	4	12 602 – 12 687	4	4
5785 – 5826	4	4	12 693 – 12 788	4	4

B. Evaluation Result

The IFCE model proposed in this article is used to evaluate the degree of impact on each channel within the absorption window, and some of the evaluation results are shown in Fig. 7.

Fig. 7 reveals that the LVWs of the absorption channels are higher at the edges of the window, except for window (b), implying that the channels located at the window edges experience greater impact, whereas the channel in the center of the absorption window is relatively less affected. In absorption windows (a), (b), and (d), the LWVs of all absorption channels range from 2 to 4, with more than 85% of the channels having LWVs between 3 and 4. This suggests that the absorption channels within these windows experience a significant impact. In contrast, absorption channels within windows (c), (e), and (f) exhibit lower LWVs, primarily ranging from 0 to 2.5, which indicates that these channels experience less impact. The results of the absorption channel evaluation are consistent with the findings depicted in Fig. 6.

The IFCE-α model, proposed in this article, was employed to assess the degree of impact on each window. In a specific CO_2 absorption window, the strong absorption channel was defined as the channel having an absorption coefficient higher than 20% of the maximum absorption coefficient. Conversely, the channel with an absorption coefficient lower than 20% of the maximum absorption coefficient was designated as a weak absorption channel. To mitigate the impact of the weak absorption channel on the window evaluation, the monitoring factor α is assigned a value of 0.5. The results of IFCE-α are presented in Table IV.

The evaluation results of the IFCE-α model indicated that 40 windows were severely affected, 17 windows were greatly affected, and 3 windows (4760–4900 cm^{-1}, 6170–6270 cm^{-1}, and 6290–6380 cm^{-1}) were slightly affected. The agreement with the expert scoring results achieved 91.7%.

The evaluation results of five windows differ from the expert scoring results, but it does not impact the usability of the windows. The 6170–6270 cm^{-1} and 6290–6380 cm^{-1} windows were assessed as "unaffected" by experts, whereas the evaluation result of the IFCE-α model was "slightly affected." This is due to the stringent constraint of the fuzzy membership function on the "unaffected" level, which enables more precise differentiation of the "unaffected" windows in practical applications, resulting in positive outcomes. The inconsistency between the assessment results of 1010–1100 cm^{-1} and 2020–2135 cm^{-1}

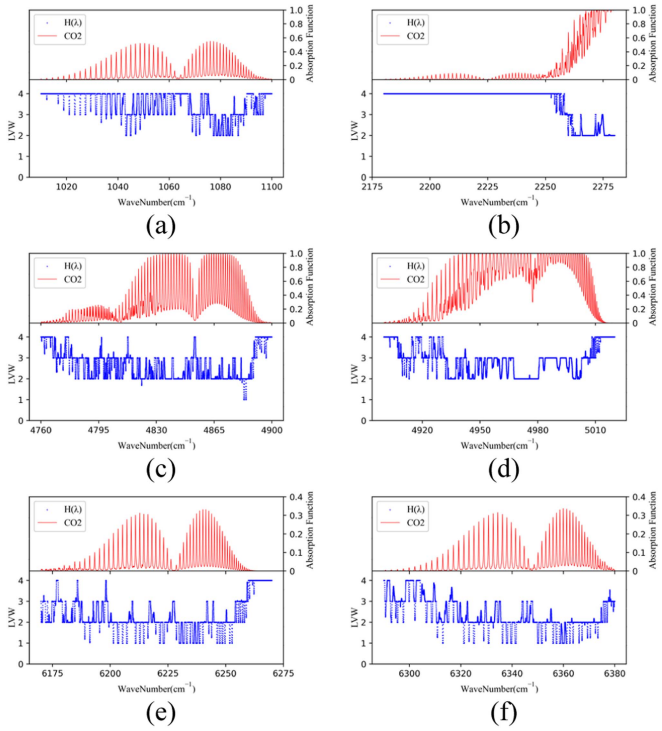

Fig. 7. Evaluation results of the absorption channels. The blue dots represent the LVWs of absorption channels, where a smaller LVW indicates a lower degree of impact on the channel. The red line represents the CO_2 absorption spectrum. (a)–(f) represent different absorption windows.

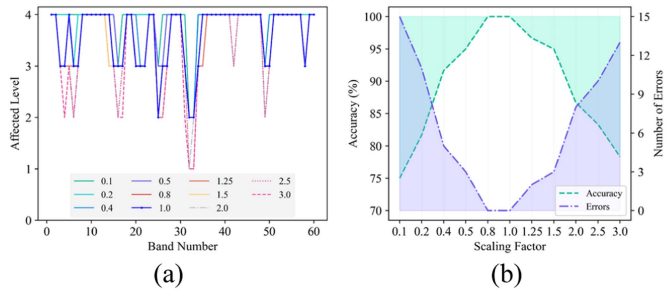

Fig. 8. Sensitivity analysis results for cut-off point values of the membership function. (a) Affected levels for each band as a function of band number and scaling factor. (b) Accuracy and number of band judgment errors as a function of scaling factor.

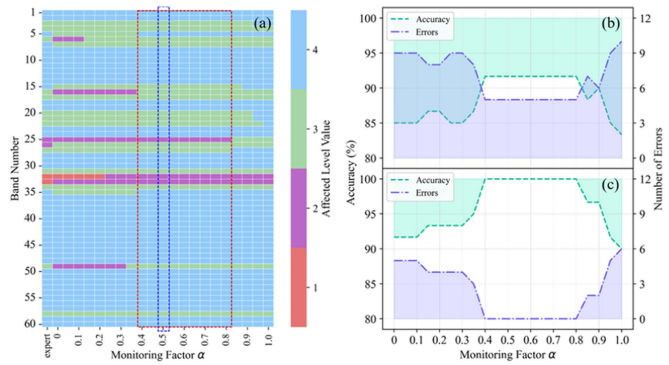

Fig. 9. Sensitivity analysis results for monitoring factor α. (a) Affected level as a function of band and supervision factor α. (b) Difference between IFCE-α results and expert scoring results as a function of the monitoring factor α. (c) Difference between IFCE-α results and the theoretical truth ($\alpha = 0.5$) as a function of the monitoring factor α.

windows and the expert assessment results is primarily attributed to the IFCE-α model's downplaying of the weak absorption channel's influence on evaluating the window grade. This leads to a reduction in impact grades. Moreover, the water vapor absorption line in the 4900–5020 cm^{-1} window is broader and exhibits greater overlap with the CO_2 absorption line, leading to a higher impact level in the evaluation compared to the expert assessment result. In practical applications, the results obtained from IFCE-α are deemed to be more reasonable.

C. Sensitivity Analysis Results for Empirical Parameters of IFCE-α Model

Performing sensitivity analysis on model parameters, such as the cut-off points of the membership function and the supervision factor α, is crucial because these values are derived from empirical knowledge.

Fig. 8(a) illustrates how the affected levels vary with the scaling factor for each band. The blue solid line represents the scenario where the cut-off point values are not scaled. When the cut-off point values are uniformly decreased (scaling factor ranging from 0.1 to 0.8), some bands exhibit increased affected level values, signifying an intensified influence; in contrast, when the cut-off point values are uniformly increased (scaling factor ranging from 1.25 to 3.0), some bands show decreased affected level values, indicating a reduced influence. Fig. 8(b) illustrates the count of bands misjudged by IFCE-α and the model's accuracy as the scaling factor varies. As the scaling factors decrease or increase, there is an increase in judgment errors and a decrease in model accuracy. If the cut-off point scaling range is $\pm 50\%$, the model accuracy can be maintained above 95%, suggesting that the IFCE-α model exhibits stability when the cut-off point value of the fuzzy membership function varies within a specific range.

We selected 20 α values evenly spaced from 0 to 1.0 and examined their influence on the evaluation outcomes. Fig. 9(a) displays the impact on 60 bands using distinct colors: the initial column illustrates the expert scoring results, while the subsequent columns depict the evaluation outcomes for various α values. The blue dashed line represents the evaluation results when α is set to 0.5, representing the theoretical baseline adopted in this study. The agreement with the expert scoring results is at its lowest when α is near 0 or 1.0, whereas it is highest when α approaches 0.5. Fig. 9(b) demonstrates that as α varies, the highest agreement with the expert scoring results is 91.7% (α ranging from 0.4 to 0.8), while the lowest is 83.3% (α equals 1.0). Referring to the theoretical baseline, depicted in Fig. 9(c), the accuracy ranges from a minimum of 90% (α equals 1.0) to 100% when α falls between 0.4 and 0.8.

TABLE V
SCENARIO PARAMETERS FOR REMOTE SENSING OBSERVATION

Parameter	Value
band	6290–6380cm^{-1}
Spectral resolution	0.1–1.2 cm^{-1}
Solar zenith angle	35.08°
Observation mode	Nadir
XCO_2	413.2 ppm
Atmospheric profile	US Standard Profile
Aerosol type	Continental average
AOD （@755nm）	0.15
Surface type	Green Grass

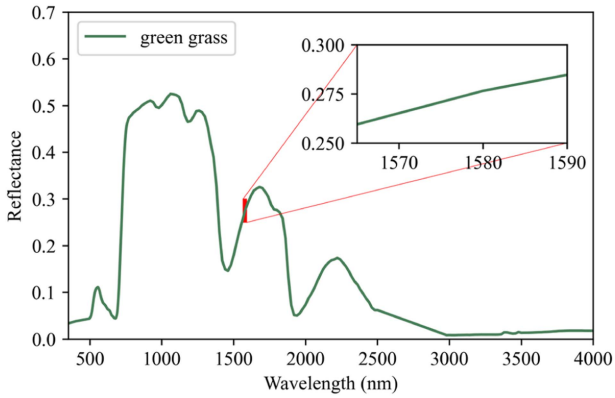

Fig. 10. Spectral albedo curve of green grass.

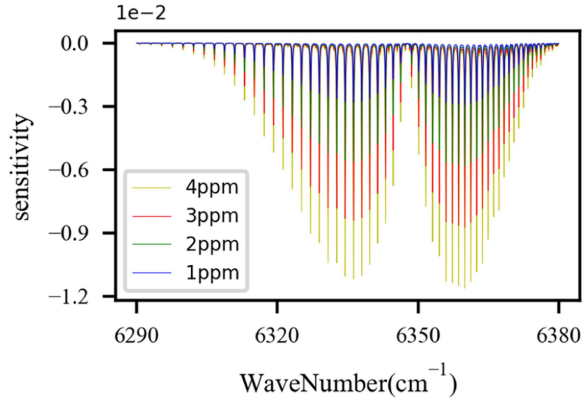

Fig. 11. Sensitivity of radiance to CO_2 column concentration changes of 1–4 ppm (the spectral resolution is assumed to be 0.1 cm^{-1}).

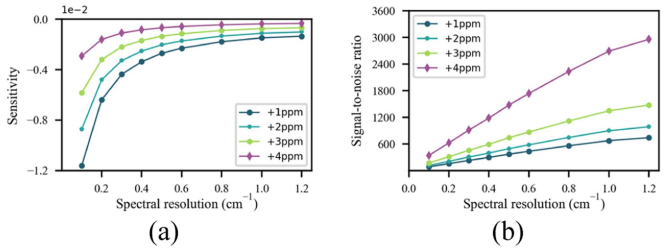

Fig. 12. Sensitivity and SNR requirements for CO_2 remote sensing detection.

D. Sensitivity Analysis Results for Radiance

This article employs the absorption window at 6290–6380 cm^{-1} for conducting radiation transfer simulations. Table V presents the main parameters of CO_2 remote sensing observation scenarios. The SZA is determined based on the sun's position during springtime in middle latitudes, with CO_2 concentration assumed to be the average value in 2020. The spectral resolution ranges from 0.1 to 1.2 cm^{-1}. Studies have indicated that in order to minimize CO_2 remote sensing detection errors, the AOD should not exceed 0.3 [54], [55]. In this case, the AOD is set to half of the maximum limit, which is 0.15. The surface reflectance is obtained from vegetation using the ASTER spectral library, as shown in Fig. 10.

In order to meet the requirements of climate change studies, the observation accuracy of XCO_2 concentration needs to be better than 1% (∼4 ppm) [56], [57]. Therefore, this article simulates the radiance when the CO_2 column concentration changes by 1–4 ppm under the assumed observation Scenario. The sensitivity of radiance to CO_2 concentration and spectral resolution was analyzed using the scene parameters given in Table V.

Fig. 11 displays the sensitivity of all channels within the 6290–6380 cm^{-1} absorption window. This indicates that the absorption of radiance by CO_2 in the 6290–6380 cm^{-1} absorption window does not reach saturation at a background concentration of 413.2 ppm, and the radiance remains highly sensitive to increasing CO_2 concentration.

TABLE VI
PARAMETERS AND VALUES FOR CONCENTRATION INVERSION

Parameter	Values
Solar zenith angle	5, 10, 15, 20, 25, 30, 35, 40, 45, 50, 55, 60
Aerosol type	Continental Average (CA), Desert, Maritime Clean (MC)
AOD(@755nm)	0.001, 0.05, 0.1, 0.15, 0.2, 0.25, 0.3
Surface type	Soil, Grass, Water

Fig. 12 illustrates the relationship among sensitivity, SNR, and spectral resolution. As spectral resolution decreases, radiance sensitivity decreases and SNR requirements increase. A detection accuracy of 3–4 ppm can be achieved when spectral resolution is 0.3 cm^{-1} and SNR is approximately 300.

E. Inversion Results

Table VI displays the scenario parameters and their corresponding values used for gas concentration inversion.

Fig. 13 illustrates the column averaging kernels at various SZAs for an AOD of 0.3 and three distinct aerosol and surface types. Similar patterns are observed in the CO_2 column averaging kernels above soil and grassland for the three distinct aerosol types. The column averaging kernel approaches unity in the troposphere (>400 hPa), and as air pressure decreases below

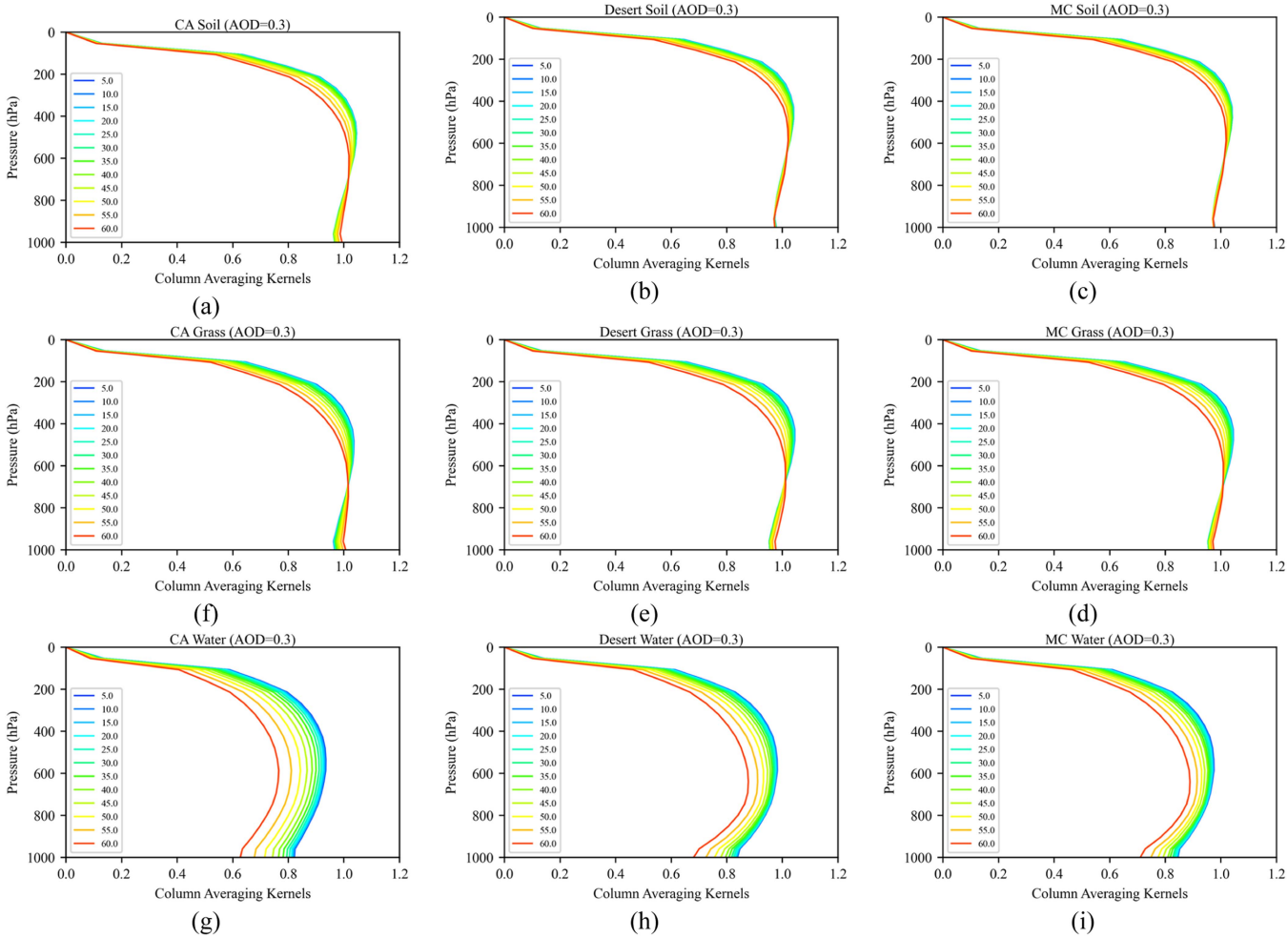

Fig. 13. CO_2 column averaging kernels at different SZAs for CA (left column), dust (middle column), and MC (right column) aerosol types over soil (top panel), grass (middle panel), and water (bottom panel).

400 hPa, it exhibits a decreasing trend and sharply drops below 200 hPa. This suggests that the 6290–6380 cm^{-1} window exhibits higher sensitivity to the tropospheric CO_2 concentration, and this sensitivity gradually diminishes with increasing altitude. The column averaging kernel above water bodies decreases near the surface ($\sim$1000 hPa). This is primarily attributed to the water body's low albedo, which leads to reduced information about the CO_2 concentration near the surface being captured in the observed irradiance.

With an increase in the SZA, the column averaging kernel shows a greater decrease with respect to elevation, indicating a reduced sensitivity of the inversion to the upper atmosphere. When the surface albedo is low, a higher SZA leads to a significant decrease in the inversion's sensitivity near the surface, as shown in Fig. 13(h) and (i).

Fig. 14 illustrates the distribution of a posteriori XCO_2 inversion errors with varying aerosol conditions, surface albedo, and SZA. The inversion results indicate that: 1) the XCO_2 inversion error increases with the SZA irrespective of the aerosol types and surface conditions. 2) The inversion errors over soil surfaces were minimal, with values consistently below 1.5 ppm for all SZAs and aerosol types. Conversely, inversion errors over water surfaces were more pronounced, reaching up to 8 ppm at higher SZAs. This outcome can be attributed to the lower inversion sensitivity over water surfaces. 3) The distribution of inversion errors on water surfaces differs significantly from that on soil and vegetation surfaces. With an increase in the AOD, the errors on soil and vegetation surfaces increase, whereas the errors on the ocean surface decrease. The influence of aerosols on XCO_2 inversion is more pronounced on surfaces with low surface albedo.

The sensitivity analysis and gas concentration inversion has determined that the 6290–6380 cm^{-1} absorption window can achieve a detection accuracy of 1–4 ppm under specific sensor configurations and observation scenarios. These findings suggest that the 6290–6380 cm^{-1} absorption window holds significant potential for detecting gas concentrations in remote sensing applications. Furthermore, the feasibility of utilizing other absorption windows in remote sensing detection can be assessed using the same approach.

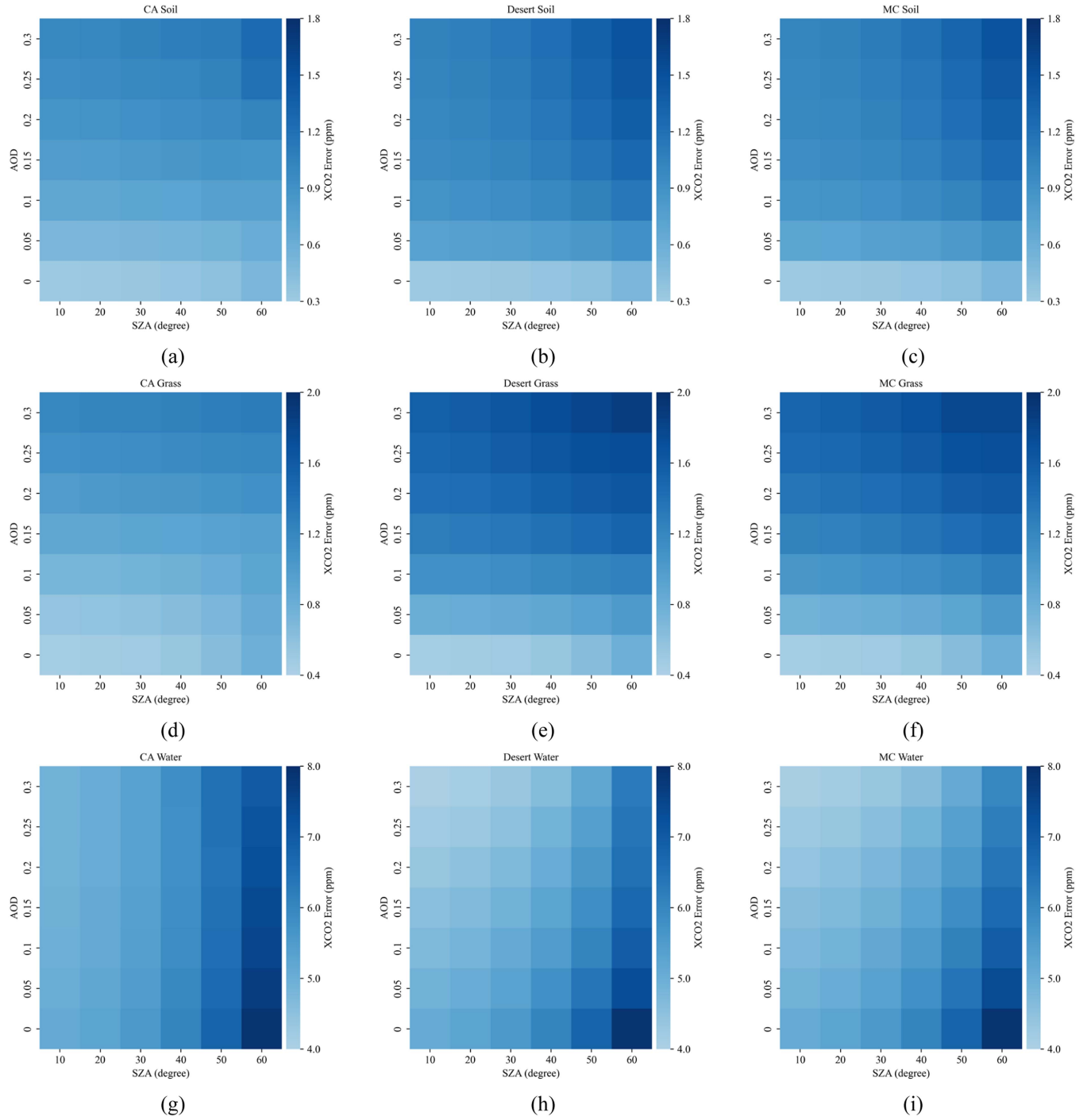

Fig. 14. A posteriori XCO_2 retrieval errors for CA (left column), dust (middle column), and MC (right column) aerosol types as a function of AODs and SZAs for soil (top panel), grass (middle panel), and water (bottom panel).

IV. Discussion

In the presence of multiple gases, various factors, including surface conditions, atmospheric elements such as aerosols and clouds, and sensor system errors such as spectral drift, can make it challenging to identify or even obscure details such as the location and intensity of target gas absorption peaks. Analyzing and studying issues, such as rapidly assessing the impact on target gas absorption characteristics across the entire spectral range and their suitability for remote sensing observations, is crucial.

Over the past two decades, band selection has relied on spectral databases and visual interpretation. This approach necessitates substantial knowledge and experience, and errors in band selection can easily occur. Furthermore, experimental results are often neither reproducible nor shareable. These challenges

arise not only during ground verification before satellite launch but also during on-orbit satellite data processing [58], [59]. To acquire effective absorption characteristics of the target gases, various methods relying on satellite-observed radiance have been extensively used to select inversion channels, such as the ratio spectrometry method [60], information content method [61], normalized sensitivity method [62], and machine learning [63]. Although this can enable high-precision inversion, it often comes at a higher cost. This article focuses on the band design phase before satellite launch and aims to investigate the absorption characteristics of the target gas unaffected by the presence of multiple interfering gases.

This article successfully establishes the technical framework for atmospheric remote sensing absorption spectral characterization, SCATF, based on the HITRAN database, an enhanced fuzzy comprehensive evaluation model, and an optimized inversion algorithm. Fuzzy membership functions, based on gas absorption intensity, are designed to analyze the extent of influence on absorption characteristics. To differentiate between the contributions of strong and weak absorption channels in the assessment of absorption windows, an enhanced fuzzy comprehensive evaluation model, IFCE-α, is developed using a monitoring factor α, and the model's robustness is demonstrated. Finally, the usability of absorption windows in atmospheric detection is assessed through sensitivity analysis and optimization inversion algorithms.

In this study, we successfully identified 60 CO_2 absorption windows in the presence of six absorptive gases. The agreement between the IFCE-α evaluation results and expert assessments reached 91.7% when using a supervisory factor α of 0.5. Five windows yielded evaluation results that differed from those of the experts. This divergence can be attributed to the strict constraints imposed by fuzzy membership functions on the "unaffected" grade, as well as variations in the IFCE-α model's emphasis on strong versus weak absorption channels. We believe that this distinction enhances the precision of rating window impact levels, thereby positively affecting window assessments. In addition, this study offers both an overall evaluation of the windows and detailed assessments of individual channels within them, which are anticipated to aid in the development of inversion algorithms.

In addition, this study performed sensitivity analyses on two empirical parameters: the membership function thresholds and the supervisory factor α. The evaluation results exhibit gradual changes with these two parameters, indicating the reliability and robustness of the IFCE-α model, which enhances the credibility of the experimental results. The evaluation results maintained 95% accuracy when the threshold scaling coefficient ranged from 0.5 to 1.5. Likewise, when α varied between 0.4 and 0.8, the evaluation results perfectly matched the theoretical true values. The evaluation results exhibit gradual changes with these two parameters, indicating the reliability and robustness of the IFCE-α model, which enhances the credibility of the experimental results.

Furthermore, this article examines the column averaging kernel and a posteriori error in CO_2 concentration inversion under varying observation scenarios using the optimal inversion algorithm. It also investigates the applicability of absorption windows in atmospheric sensing through the integration of radiance sensitivity and SNR. The inversion results of the a posteriori error are consistent with previous studies [54], [64], [65]. Nonetheless, employing the column-averaged kernel to depict the inversion sensitivity of CO_2 at varying altitudes in this study elucidates the impact of observation scenario parameters on the inversion process, aiding in error attribution.

Besides, there are two points that need attention: 1) the construction of fuzzy membership functions is a creative task that requires consideration of practical problems. The boundary points of the membership functions are not uniquely determined and can be obtained through empirical reasoning, statistical experiments, and other methods. In addition, approximate membership functions can also be established and gradually improved through continuous learning. In this study, the fuzzy membership functions are constructed based on the intensity of absorption spectra. Future work will attempt to construct different fuzzy membership functions and analyze their impact on the evaluation results. 2) The monitoring factor α enables the IFCE-α model to distinguish the importance of strong and weak absorption channels and there is still room for optimization in determining the value of α. In this study, α is manually set, introducing some subjectivity. Future work will focus on establishing an optimization mechanism to achieve automatic optimization of α, reducing human intervention and enhancing the objectivity of window evaluation.

V. Conclusion

With the growing need for atmospheric composition monitoring, the utilization of atmospheric remote sensing technology employing molecular absorption spectroscopy assumes an indispensable role. This technology also imposes more stringent requirements on the quantitative analysis of gas absorption spectral characteristics and the simulation of radiative transfer within absorption windows. However, the assessment and interpretation of spectral characteristics related to target gases, especially in the presence of multiple interfering absorbing gases, still pose significant challenges. Furthermore, the technical intricacies involved in the quantitative analysis of spectral characteristics and the simulation of radiative transfer within absorption windows require additional clarification.

This article presents a technical framework called spectrum characteristics analysis technical framework (SCATF) and provides a comprehensive description of the specific methodologies and procedures used to enable the quantitative analysis of spectral characteristics and the simulation of radiative transfer within absorption windows.

In summary, the SCATF framework accurately extracts the absorption characteristics of the target gas and rapidly evaluates the impact on absorption channels and windows. In addition, it provides insights into the performance of absorption windows in remote sensing detection, offering a novel approach for designing detection bands in atmospheric remote sensing.

APPENDIX A

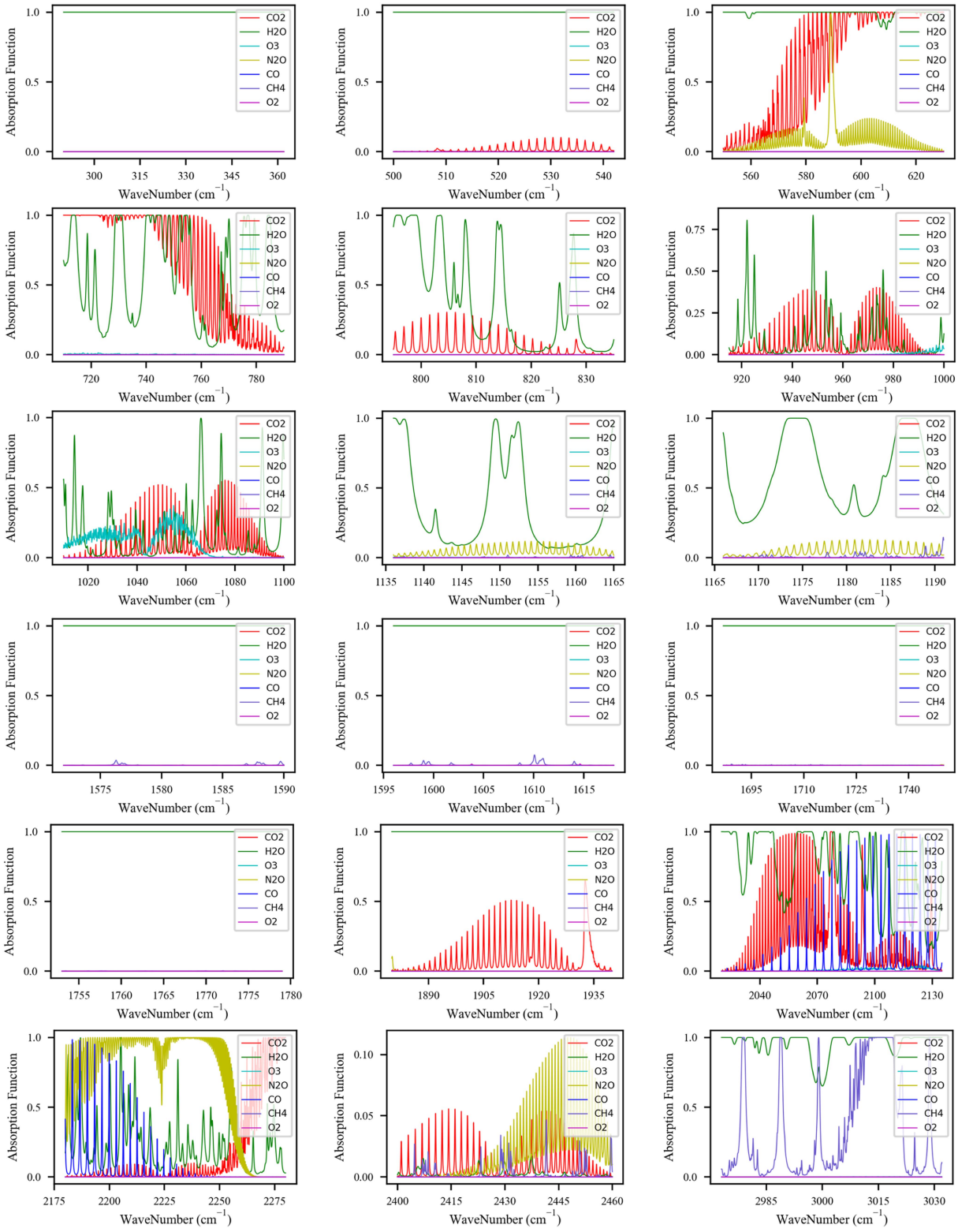

Fig. 15. Absorption spectra of 7 gases within the CO_2 absorption windows.

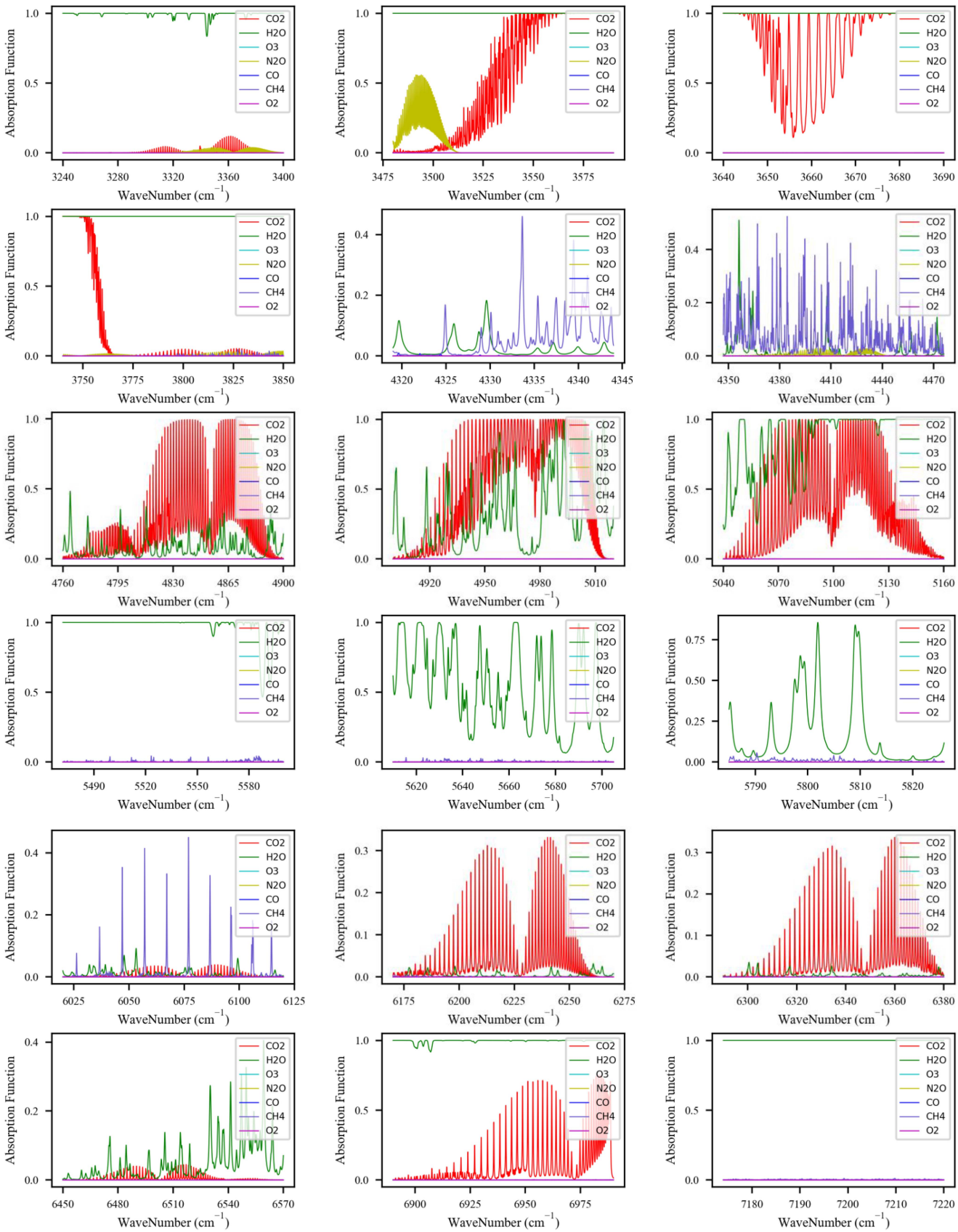

Fig. 15. *(Continued.)*

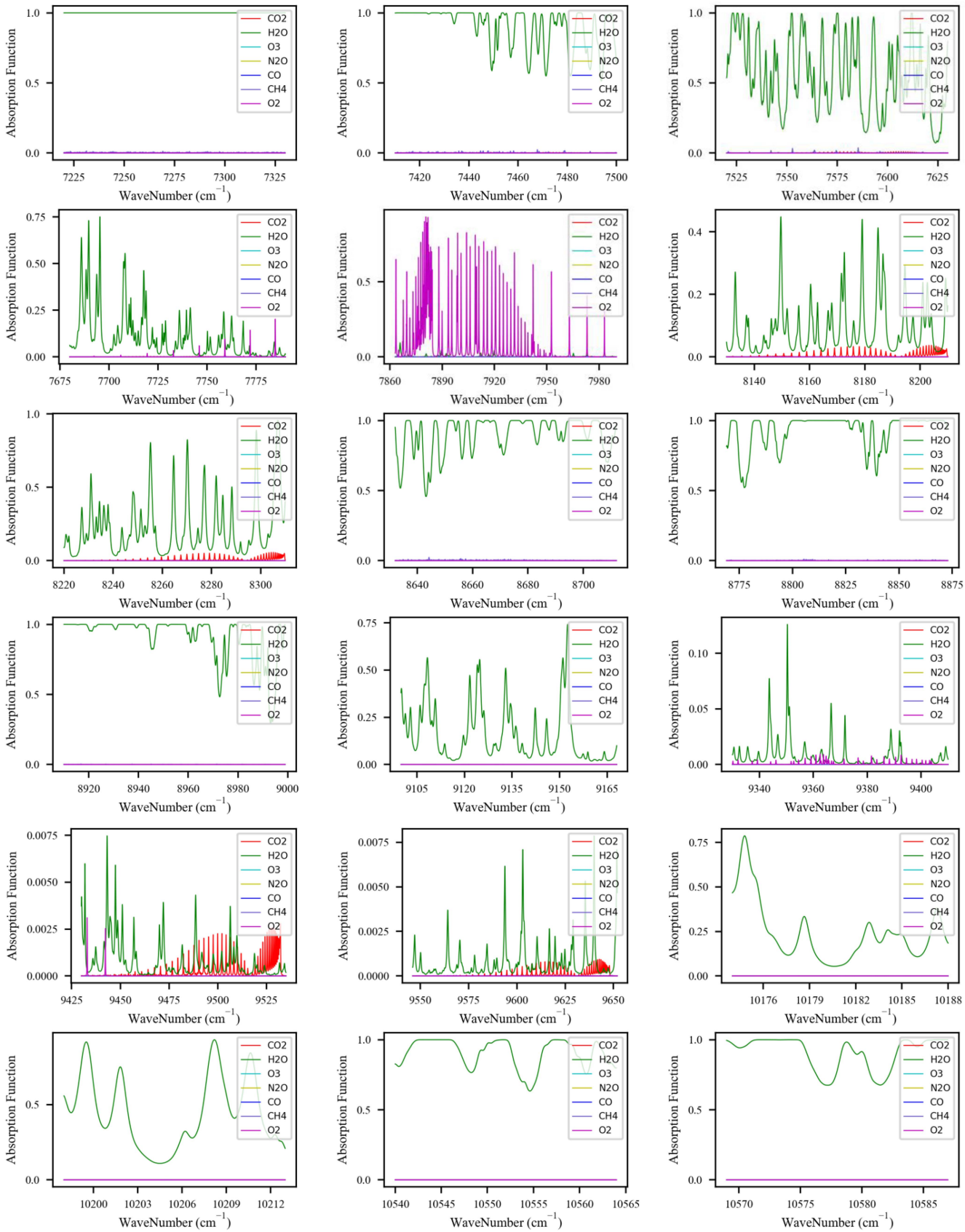

Fig. 15. *(Continued.)*

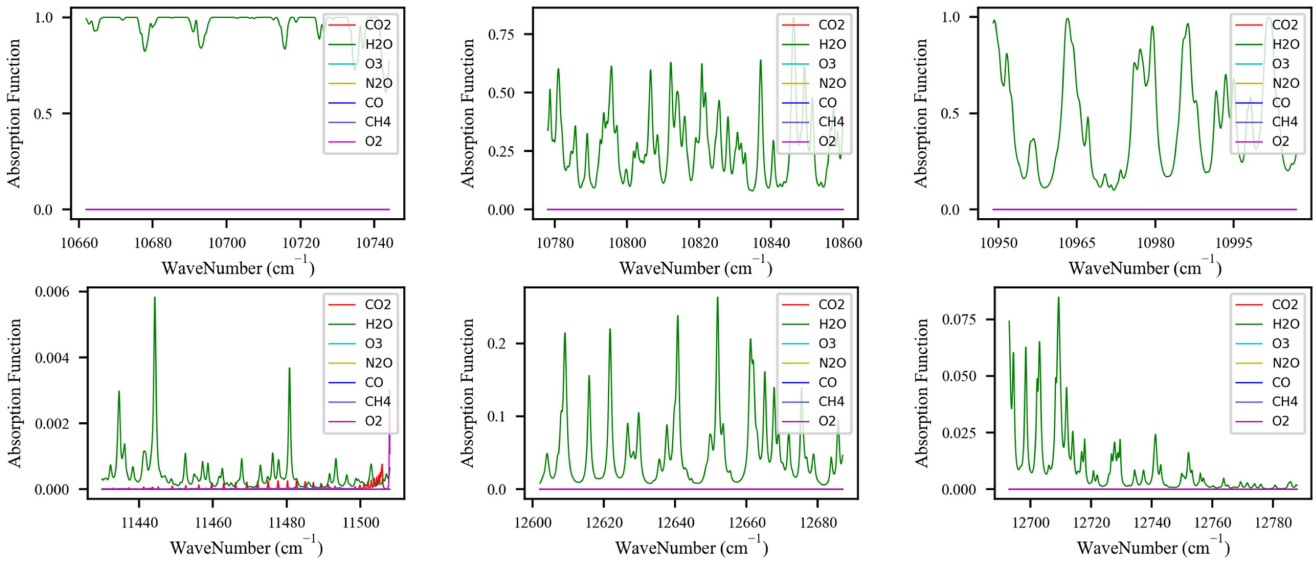

Fig. 15. *(Continued.)*

Acknowledgment

The authors would like to thank A. Rozanov for supplying the radiative transfer model SCIATRAN. N. HITRAN data were obtained from the HITRAN on the web at https://hitran.iao.ru/ accessed on Feb. 2, 2023.

References

[1] I. Leifer et al., "Remote sensing and in situ measurements of methane and ammonia emissions from a megacity dairy complex: Chino, CA," *Environ. Pollut.*, vol. 221, pp. 37–51, Feb. 2017, doi: 10.1016/j.envpol.2016.09.083.

[2] S. Yu et al., "Photon-counting distributed free-space spectroscopy," *Light Sci. Appl.*, vol. 10, no. 1, Oct. 2021, Art. no. 212, doi: 10.1038/s41377-021-00650-2.

[3] Q. Zhang, Y. Chen, and Y. Liu, "Study on the online detection of atmospheric sulfur via laser-induced breakdown spectroscopy," *J. Anal. At. Spectrometry*, vol. 36, no. 5, pp. 1028–1033, Mar. 2021, doi: 10.1039/D1JA00017A.

[4] B. Zhang et al., "Progress and challenges in intelligent remote sensing satellite systems," *IEEE J. Sel. Topics Appl. Earth Observ. Remote Sens.*, vol. 15, pp. 1814–1822, 2022, doi: 10.1109/JSTARS.2022.3148139.

[5] W. W. Su, C. Boulet, C. A. Almodovar, Y. Ding, C. L. Strand, and R. K. Hanson, "Line mixing study on the fundamental rovibrational band of nitric oxide near 5.3 μm," *J. Quant. Spectrosc. Radiative Transfer*, vol. 278, Feb. 2022, Art. no. 107997.

[6] W. W. Su, Y. Ding, C. L. Strand, and R. K. Hanson, "Line mixing study of carbon monoxide near 4.7 μm broadened by nitrogen, helium, and hydrogen," *J. Mol. Spectrosc.*, vol. 390, Nov./Dec. 2022, Art. no. 111699.

[7] T. A. Odintsova, E. Fasci, S. Gravina, L. Gianfrani, and A. Castrillo, "Optical feedback laser absorption spectroscopy of N_2O at 2 µm," *J. Quant. Spectrosc. Radiative Transfer*, vol. 254, Oct. 2020, Art. no. 107190.

[8] R. R. Gamache, R. Lynch, and S. P. Neshyba, "New developments in the theory of pressure-broadening and pressure-shifting of spectral lines of H_2O: The complex Robert-Bonamy formalism," *J. Quant. Spectrosc. Radiative Transfer*, vol. 59, no. 3/5, pp. 319–335, Mar./May 1998, doi: 10.1016/S0022-4073(97)00123-4.

[9] H. Tran, C. Boulet, S. Stefani, M. Snels, and G. Piccioni, "Measurements and modelling of high pressure pure CO_2 spectra from 750 to 8500 cm^{-1}. I—Central and wing regions of the allowed vibrational bands," *J. Quant. Spectrosc. Radiative Transfer*, vol. 112, no. 6, pp. 925–936, Apr. 2011, doi: 10.1016/j.jqsrt.2010.11.021.

[10] B. Maté, C. Lugez, G. T. Fraser, and W. J. Lafferty, "Absolute intensities for the O_2 1.27 μm continuum absorption," *J. Geophys. Res. Atmos.*, vol. 104, no. D23, pp. 30585–30590, Dec. 1999, doi: 10.1029/1999JD900824.

[11] D. Jacquemart, F. Gueye, O. M. Lyulin, E. V. Karlovets, D. Baron, and V. I. Perevalov, "Infrared spectroscopy of CO_2 isotopologues from 2200 to 7000 cm^{-1}: I—Characterizing experimental uncertainties of positions and intensities," *J. Quant. Spectrosc. Radiative Transfer*, vol. 113, no. 11, pp. 961–975, Jul. 2012, doi: 10.1016/j.jqsrt.2012.02.020.

[12] K. Owen, E. T. Es-sebbar, and A. Farooq, "Measurements of NH_3 linestrengths and collisional broadening coefficients in N_2, O_2, CO_2, and H_2O near 1103.46 cm^{-1}," *J. Quant. Spectrosc. Radiative Transfer*, vol. 121, pp. 56–68, May 2013, doi: 10.1016/j.jqsrt.2013.02.001.

[13] H. Tran, J. Vander Auwera, T. Bertin, W. Fakhardji, O. Pirali, and J. M. Hartmann, "Absorption of methane broadened by carbon dioxide in the 3.3 μm spectral region: From line centers to the far wings," *Icarus*, vol. 384, Sep. 2022, Art. no. 115093.

[14] C. Sousa-Silva, J. J. Petkowski, and S. Seager, "Molecular simulations for the spectroscopic detection of atmospheric gases," *Phys. Chem. Chem. Phys.*, vol. 21, no. 35, pp. 18970–18987, Aug. 2019, doi: 10.1039/C8CP07057A.

[15] E. J. Mlawer, V. H. Payne, J. L. Moncet, J. S. Delamere, M. J. Alvarado, and D. C. Tobin, "Development and recent evaluation of the MT_CKD model of continuum absorption," *Philos. Trans. Roy. Soc. A, Math. Phys. Eng. Sci.*, vol. 370, no. 1968, pp. 2520–2556, Jun. 2012, doi: 10.1098/rsta.2011.0295.

[16] C. M. Western, "PGOPHER: A program for simulating rotational, vibrational and electronic spectra," *J. Quant. Spectrosc. Radiative Transfer*, vol. 186, pp. 221–242, Jan. 2017, doi: 10.1016/j.jqsrt.2016.04.010.

[17] T. Furtenbacher and A. G. Csaszar, "MARVEL: Measured active rotational-vibrational energy levels. II. Algorithmic improvements," *J. Quant. Spectrosc. Radiative Transfer*, vol. 113, no. 11, pp. 929–935, Jul. 2012, doi: 10.1016/j.jqsrt.2012.01.005.

[18] J. Tennyson et al., "The 2020 release of the ExoMol database: Molecular line lists for exoplanet and other hot atmospheres," *J. Quant. Spectrosc. Radiative Transfer*, vol. 255, Nov. 2020, Art. no. 107228.

[19] L. S. Rothman et al., "HITEMP, the high-temperature molecular spectroscopic database," *J. Quant. Spectrosc. Radiative Transfer*, vol. 111, no. 15, pp. 2139–2150, Oct. 2010, doi: 10.1016/j.jqsrt.2010.05.001.

[20] P. M. Chu, F. R. Guenther, G. C. Rhoderick, and W. J. Lafferty, "The NIST quantitative infrared database," *J. Res. Nat. Inst. Standards Technol.*, vol. 104, no. 1, pp. 59–81, Jan./Feb. 1999, doi: 10.6028/jres.104.004.

[21] S. W. Sharpe, T. J. Johnson, R. L. Sams, P. M. Chu, G. C. Rhoderick, and P. A. Johnson, "Gas-phase databases for quantitative infrared spectroscopy," *Appl. Spectrosc.*, vol. 58, no. 12, pp. 1452–1461, Jul. 2004.

[22] S. E. Qian, "Hyperspectral satellites, evolution, and development history," *IEEE J. Sel. Topics Appl. Earth Observ. Remote Sens.*, vol. 14, pp. 7032–7056, 2021, doi: 10.1109/JSTARS.2021.3090256.

[23] C. Xing et al., "Identifying the wintertime sources of volatile organic compounds (VOCs) from MAX-DOAS measured formaldehyde and glyoxal in Chongqing, Southwest China," *Sci. Total Environ.*, vol. 715, May 2020, Art. no. 136258.

[24] J. Heymann et al., "SCIAMACHY WFM-DOAS XCO_2: Comparison with CarbonTracker XCO_2 focusing on aerosols and thin clouds," *Atmos. Meas. Tech.*, vol. 5, no. 8, pp. 1935–1952, Aug. 2012, doi: 10.5194/amt-5-1935-2012.

[25] S. Oshchepkov et al., "Effects of atmospheric light scattering on spectroscopic observations of greenhouse gases from space. Part 2: Algorithm intercomparison in the GOSAT data processing for CO_2 retrievals over TCCON sites," *J. Geophys. Res. Atmos.*, vol. 118, no. 3, pp. 1493–1512, Jan. 2013, doi: 10.1002/jgrd.50146.

[26] R. V. Kochanov, I. E. Gordon, L. S. Rothman, P. Wcisło, C. Hill, and J. S. W. Ilzewski, "HITRAN application programming interface (HAPI): A comprehensive approach to working with spectroscopic data," *J. Quant. Spectrosc. Radiative Transfer*, vol. 177, pp. 15–30, Jul. 2016, doi: 10.1016/j.jqsrt.2016.03.005.

[27] C. S. Goldenstein, V. A. Miller, R. M. Spearrin, and C. L. Strand, "SpectraPlot.com: Integrated spectroscopic modeling of atomic and molecular gases," *J. Quant. Spectrosc. Radiative Transfer*, vol. 200, pp. 249–257, Oct. 2017, doi: 10.1016/j.jqsrt.2017.06.007.

[28] E. Pannier and C. O. Laux, "RADIS: A nonequilibrium line-by-line radiative code for CO_2 and HITRAN-like database species," *J. Quant. Spectrosc. Radiative Transfer*, vol. 222, pp. 12–25, Jan. 2019, doi: 10.1016/j.jqsrt.2018.09.027.

[29] C. M. Murzyn, E. R. Jans, and M. D. Clemenson, "Spears: A database-invariant spectral modeling API," *J. Quant. Spectrosc. Radiative Transfer*, vol. 277, Jan. 2022, Art. no. 107958.

[30] H. K. Chan, X. Sun, and S. H. Chung, "When should fuzzy analytic hierarchy process be used instead of analytic hierarchy process?," *Decis. Support Syst.*, vol. 125, Oct. 2019, Art. no. 113114.

[31] E. K. Zavadskas, A. Mardani, Z. Turskis, A. Jusoh, and K. M. Nor, "Development of TOPSIS method to solve complicated decision-making problems—An overview on developments from 2000 to 2015," *Int. J. Inf. Technol. Decis. Mak.*, vol. 15, no. 3, pp. 645–682, May 2016, doi: 10.1142/S0219622016300019.

[32] F. Sarraf and S. H. Nejad, "Improving performance evaluation based on balanced scorecard with grey relational analysis and data envelopment analysis approaches: Case study in water and wastewater companies," *Eval. Prog. Plan.*, vol. 79, Apr. 2020, Art. no. 101762.

[33] Z. Wang, J. Wang, D. Yu, and K. Chen, "The potential evaluation of groundwater by integrating rank sum ratio (RSR) and machine learning algorithms in the Qaidam Basin," *Environ. Sci. Pollut. Res.*, vol. 30, pp. 63991–64005, Apr. 2023, doi: 10.1007/s11356-023-26961-y.

[34] X. Wu and F. Hu, "Analysis of ecological carrying capacity using a fuzzy comprehensive evaluation method," *Ecol. Indicators*, vol. 113, Jun. 2020, Art. no. 106243.

[35] P. Yi, Q. Dong, W. Li, and L. Wang, "Measurement of city sustainability based on the grey relational analysis: The case of 15 sub-provincial cities in China," *Sustain. Cities Soc.*, vol. 73, Oct. 2021, Art. no. 103143.

[36] I. E. Gordon et al., "The HITRAN2020 molecular spectroscopic database," *J. Quant. Spectrosc. Radiative Transfer*, vol. 277, Jan. 2022, Art. no. 107949.

[37] A. Berk and F. Hawes, "Validation of MODTRAN 6 and its line-by-line algorithm," *J. Quant. Spectrosc. Radiative Transfer*, vol. 203, pp. 542–556, Dec. 2017, doi: 10.1016/j.jqsrt.2017.03.004.

[38] M. J. Alvarado et al., "Performance of the line-by-line radiative transfer model (LBLRTM) for temperature, water vapor, and trace gas retrievals: Recent updates evaluated with IASI case studies," *Atmos. Chem. Phys.*, vol. 13, no. 14, pp. 6687–6711, Jul. 2013, doi: 10.5194/acp-13-6687-2013.

[39] V. V. Rozanov, T. Dinter, A. V. Rozanov, A. Wolanin, A. Bracher, and J. P. Burrows, "Radiative transfer modeling through terrestrial atmosphere and ocean accounting for inelastic processes: Software package SCIATRAN," *J. Quant. Spectrosc. Radiative Transfer*, vol. 194, pp. 65–85, Jun. 2017, doi: 10.1016/j.jqsrt.2017.03.009.

[40] Y.-H. Kao, P. C.-P. Chao, and C.-L. Wey, "Design and validation of a new PPG module to acquire high-quality physiological signals for high-accuracy biomedical sensing," *IEEE J. Sel. Topics Quantum Electron.*, vol. 25, no. 1, Jan./Feb. 2019, Art. no. 69000210, doi: 10.1109/JSTQE.2018.2871604.

[41] D. Wunch et al., "Calibration of the total carbon column observing network using aircraft profile data," *Atmos. Meas. Tech.*, vol. 3, no. 5, pp. 1351–1362, Oct. 2010, doi: 10.5194/amt-3-1351-2010.

[42] D. Wunch et al., "The total carbon column observing network," *Philos. Trans. Roy. Soc. A*, vol. 369, no. 1943, pp. 2087–2112, May 2011, doi: 10.1098/rsta.2010.0240.

[43] B. Barret, Y. Gouzenes, E. Le Flochmoen, and S. Ferrant, "Retrieval of Metop-A/IASI N_2O profiles and validation with NDACC FTIR data," *Atmosphere*, vol. 12, no. 2, Feb. 2021, Art. no. 219, doi: 10.3390/atmos12020219.

[44] R. Chalinel et al., "Evaluation and global-scale observation of nitrous oxide from IASI on Metop-A," *Remote Sens.*, vol. 14, no. 6, Mar. 2022, Art. no. 1403, doi: 10.3390/rs14061403.

[45] R. A. Minzner, "The 1976 standard atmosphere and its relationship to earlier standards," *Rev. Geophys.*, vol. 15, no. 3, pp. 375–384, Aug. 1977, doi: 10.1029/RG015i003p00375.

[46] C. Mattar, C. Durán-Alarcón, J. C. Jiménez-Muñoz, A. Santamaría-Artigas, L. Olivera-Guerra, and J. A. Sobrino, "Global atmospheric profiles from reanalysis information (GAPRI): A new database for earth surface temperature retrieval," *Int. J. Remote Sens.*, vol. 36, no. 19/20, pp. 5045–5060, Jun. 2015, doi: 10.1080/01431161.2015.1054965.

[47] J. Lee et al., "Characteristics of aerosol types from AERONET sunphotometer measurements," *Atmos. Environ.*, vol. 44, no. 26, pp. 3110–3117, Aug. 2010, doi: 10.1016/j.atmosenv.2010.05.035.

[48] P. Koepke, J. Gasteiger, and M. Hess, "Optical properties of desert aerosol with non-spherical mineral particles: Data incorporated to OPAC," *Atmos. Chem. Phys.*, vol. 15, no. 10, pp. 5947–5956, May 2015, doi: 10.5194/acp-15-5947-2015.

[49] H. Emami, B. Mojaradi, and A. Safari, "A new approach for land surface emissivity estimation using LDCM data in semi-arid areas: Exploitation of the ASTER spectral library data set," *Int. J. Remote Sens.*, vol. 37, no. 21, pp. 5060–5085, Sep. 2016, doi: 10.1080/01431161.2016.1226524.

[50] G. Forestier, J. Inglada, C. Wemmert, and P. Gançarski, "Comparison of optical sensors discrimination ability using spectral libraries," *Int. J. Remote Sens.*, vol. 34, no. 7, pp. 2327–2349, Dec. 2013, doi: 10.1080/01431161.2012.744488.

[51] C. D. Rodgers, "Optimal methods for nonlinear inverse problems," in *Inverse Methods for Atmospheric Sounding: Theory and Practice*. Singapore: World Scientific, 2000, pp. 81–100.

[52] C. W. O'Dell et al., "The ACOS CO_2 retrieval algorithm–Part 1: Description and validation against synthetic observations," *Atmos. Meas. Tech.*, vol. 5, no. 1, pp. 99–121, Jan. 2012, doi: 10.5194/amt-5-99-2012.

[53] K. Sang, G. L. Fontana, and S. E. Piovan, "Assessing railway landscape by AHP process with GIS: A study of the Yunnan-Vietnam railway," *Remote Sens.*, vol. 14, no. 3, Jan. 2022, Art. no. 603, doi: 10.3390/rs14030603.

[54] S. Sanghavi, R. Nelson, C. Frankenberg, and M. Gunson, "Aerosols in OCO-2/GOSAT retrievals of XCO_2: An information content and error analysis," *Remote Sens. Environ.*, vol. 251, Dec. 2020, Art. no. 112053.

[55] T. E. Taylor et al., "Orbiting carbon observatory-2 (OCO-2) cloud screening algorithms: Validation against collocated MODIS and CALIOP data," *Atmos. Meas. Tech.*, vol. 9, no. 3, pp. 973–989, Mar. 2016, doi: 10.5194/amt-9-973-2016.

[56] C. E. Miller et al., "Precision requirements for space-based data," *J. Geophys. Res. Atmos.*, vol. 112, no. D10, May 2007, Art. no. D10314, doi: 10.1029/2006JD007659.

[57] C. He, M. Ji, M. L. Grieneisen, and Y. Zhan, "A review of datasets and methods for deriving spatiotemporal distributions of atmospheric CO_2," *J. Environ. Manage.*, vol. 322, Nov. 2022, Art. no. 116101.

[58] D. Di, J. Li, W. Han, and R. Yin, "Geostationary hyperspectral infrared sounder channel selection for capturing fast-changing atmospheric information," *IEEE Trans. Geosci. Remote Sens.*, vol. 60, 2022, Art. no. 4102210, doi: 10.1109/TGRS.2021.3078829.

[59] W. L. Smith et al., "Hyperspectral satellite radiance atmospheric profile information content and its dependence on spectrometer technology," *IEEE J. Sel. Topics Appl. Earth Observ. Remote Sens.*, vol. 14, pp. 4720–4736, 2021, doi: 10.1109/JSTARS.2021.3073482.

[60] H. H. Ye et al., "Study of the effect of surface reflectance on atmospheric CO_2 retrieval and ratio spectrometry," *Spectrosc. Spectral Anal.*, vol. 33, no. 8, pp. 2182–2187, Aug. 2013, doi: 10.3964/j.issn.1000-0593(2013)08-2182-06.

[61] Y. Villalobos, P. Rayner, S. Thomas, and J. Silver, "The potential of orbiting carbon observatory-2 data to reduce the uncertainties in CO_2 surface fluxes over Australia using a variational assimilation scheme," *Atmos. Chem. Phys.*, vol. 20, no. 14, pp. 8473–8500, Jul. 2020, doi: 10.5194/acp-20-8473-2020.

[62] L. Zhao, S. Chen, Y. Xue, and T. Cui, "Study of atmospheric carbon dioxide retrieval method based on normalized sensitivity," *Remote Sens.*, vol. 14, no. 5, Feb. 2022, Art. no. 1106, doi: 10.3390/rs14051106.

[63] M. Chen, L. Ni, X. Jiang, and H. Wu, "Retrieving atmospheric and land surface parameters from at-sensor thermal infrared hyperspectral data with artificial neural network," *IEEE J. Sel. Topics Appl. Earth Observ. Remote Sens.*, vol. 12, no. 7, pp. 2409–2416, Jul. 2019, doi: 10.1109/JSTARS.2019.2904992.

[64] P. Rong et al., "Sensitivity analysis of an XCO_2 retrieval algorithm for high-resolution short-wave infrared spectra," *Optik*, vol. 209, May 2020, Art. no. 164502, doi: 10.1016/j.ijleo.2020.164502.

[65] X. Chen et al., "A theoretical analysis for improving aerosol-induced CO_2 retrieval uncertainties over land based on TanSat Nadir observations under clear sky conditions," *Remote Sens.*, vol. 11, no. 9, May 2019, Art. no. 1061, doi: 10.3390/rs11091061.

Zhaocong Wu received the B.S. and Ph.D. degrees in photogrammetry and remote sensing techniques from Wuhan University, Wuhan, China, in 1986 and 2004, respectively.

He is a Professor with the School of Remote Sensing and Information Engineering, Wuhan University. His research interests include atmospheric remote sensing, radiative transfer, high-resolution image processing, image analysis, and pattern recognition.

Mingliang Li received the B.S. degree in remote sensing science and technology and the M.S. degree in photogrammetry and remote sensing from the School of Information Science and Engineering, Shandong Agricultural University, Tai'an, China, in 2014 and 2017, respectively. He is currently working toward the Ph.D. degree in photogrammetry and remote sensing with Wuhan University, Wuhan, China.

His research interests include atmospheric remote sensing, radiative transfer, and quantitative inversion.

Keyi Rao is currently working toward the combined master's and Ph.D. degree in remote sensing science and technology with the School of Remote Sensing and Information Engineering, Wuhan University, Wuhan, China.

Her research interests include preprocessing and application of hyperspectral remote sensing images, as well as inland water environment monitoring with remote sensing.

Yixian Yue received the B.S. degree in remote sensing science and technology in 2022 from Wuhan University, Wuhan, China, where she is currently working toward the M.S. degree in resources and environment with the School of Remote Sensing and Information Engineering, Wuhan University, Wuhan, China.

Her research interest focuses on the quantitative remote sensing of vegetation.

Anquan Xia received the B.S. degree in remote sensing science and technology and the M.S. degree in photogrammetry and remote sensing from the School of Information Science and Engineering, Shandong Agricultural University, Tai'an, China, in 2014 and 2017, respectively. He is currently working toward the Ph.D. degree in ecology with the University of Chinese Academy of Sciences, Beijing, China.

His research interests include soil organic carbon estimation and soil carbon sink in Himalaya and Tibetan plateau grassland.